nature

https://doi.org/10.1038/s41586-022-04474-x

Accelerated Article Preview

Altered TMPRSS2 usage by SARS-CoV-2 Omicron impacts tropism and fusogenicity

Received: 21 December 2021

Accepted: 26 January 2022

Accelerated Article Preview

Cite this article as: Meng, B. et al. Altered TMPRSS2 usage by SARS-CoV-2 Omicron impacts tropism and fusogenicity. *Nature* https://doi.org/10.1038/s41586-022-04474-x (2022).

Bo Meng, Adam Abdullahi, Isabella A. T. M. Ferreira, Niluka Goonawardane, Akatsuki Saito, Izumi Kimura, Daichi Yamasoba, Pehuén Pereyra Gerber, Saman Fatihi, Surabhi Rathore, Samantha K. Zepeda, Guido Papa, Steven A. Kemp, Terumasa Ikeda, Mako Toyoda, Toong Seng Tan, Jin Kuramochi, Shigeki Mitsunaga, Takamasa Ueno, Kotaro Shirakawa, Akifumi Takaori-Kondo, Teresa Brevini, Donna L. Mallery, Oscar J. Charles, CITIID-NIHR BioResource COVID-19 Collaboration*, The Genotype to Phenotype Japan (GP-Japan) Consortium*, Ecuador-COVID19 Consortium*, John E. Bowen, Anshu Joshi, Alexandra C. Walls, Laurelle Jackson, Darren Martin, Kenneth G. C. Smith, John Bradley, John A. G. Briggs, Jinwook Choi, Elo Madissoon, Kerstin Meyer, Petra Mlcochova, Lourdes Ceron-Gutierrez, Rainer Doffinger, Sarah A. Teichmann, Andrew J. Fisher, Matteo S. Pizzuto, Anna de Marco, Davide Corti, Myra Hosmillo, Joo Hyeon Lee, Leo C. James, Lipi Thukral, David Veesler, Alex Sigal, Fotios Sampaziotis, Ian G. Goodfellow, Nicholas J. Matheson, Kei Sato & Ravindra K. Gupta

This is a PDF file of a peer-reviewed paper that has been accepted for publication. Although unedited, the content has been subjected to preliminary formatting. Nature is providing this early version of the typeset paper as a service to our authors and readers. The text and figures will undergo copyediting and a proof review before the paper is published in its final form. Please note that during the production process errors may be discovered which could affect the content, and all legal disclaimers apply.

ACCELERATED ARTICLE PREVIEW

Altered TMPRSS2 usage by SARS-CoV-2 Omicron impacts tropism and fusogenicity

Bo Meng[1,2,44], Adam Abdullahi[1,2,44], Isabella A.T.M. Ferreira[1,2,44], Niluka Goonawardane [1,2,44] Akatsuki Saito[3,44], Izumi Kimura[4,44], Daichi Yamasoba[4,44], Pehuén Pereyra Gerber[1,2], Saman Fatihi[5], Surabhi Rathore[5], Samantha K Zepeda[6], Guido Papa[7], Steven A. Kemp[1,2], Terumasa Ikeda[8], Mako Toyoda[9], Toong Seng Tan[9], Jin Kuramochi[10], Shigeki Mitsunaga[11], Takamasa Ueno[9], Kotaro Shirakawa[11], Akifumi Takaori-Kondo[11], Teresa Brevini[2], Donna L. Mallery[7], Oscar J. Charles[12], CITIID-NIHR BioResource COVID-19 Collaboration*, The Genotype to Phenotype Japan (G2P-Japan) Consortium*, Ecuador-COVID19 Consortium*, John E Bowen[6], Anshu Joshi[6], Alexandra C. Walls[6,23], Laurelle Jackson[13], Darren Martin[14], Kenneth G.C. Smith[1,2], John Bradley[2], John A. G. Briggs[15], Jinwook Choi[16], Elo Madissoon[17,18], Kerstin Meyer[17], Petra Mlcochova[1,2], Lourdes Ceron-Gutierrez[19], Rainer Doffinger[19], Sarah A. Teichmann[17,20], Andrew J. Fisher[21], Matteo S. Pizzuto[22], Anna de Marco[22], Davide Corti[22], Myra Hosmillo[23], Joo Hyeon Lee[16,24], Leo C. James[7], Lipi Thukral[6], David Veesler[6,25], Alex Sigal[14,26], Fotios Sampaziotis[1,2,16,19], Ian G Goodfellow[23], Nicholas J. Matheson[1,2,19,27], Kei Sato[4,28]† & Ravindra K. Gupta[1,2,13]†

[1]Cambridge Institute of Therapeutic Immunology & Infectious Disease (CITIID), Cambridge, UK.
[2]Department of Medicine, University of Cambridge, Cambridge, UK.
[3]Department of Veterinary Science, Faculty of Agriculture, University of Miyazaki, Miyazaki 8892192, Japan.
[4]Division of Systems Virology, Department of Infectious Disease Control, International Research Center for Infectious Diseases, The Institute of Medical Science, The University of Tokyo, Tokyo, 1088639, Japan.
[5]CSIR Institute of Genomics and Integrative Biology, Delhi, India.
[6]Department of Biochemistry, University of Washington, Seattle, 98195 USA.
[7]MRC – Laboratory of Molecular Biology, Cambridge, UK.
[8]Division of Infection and Immunity, Joint Research Center for Human Retrovirus infection, Kumamoto University, Kumamoto 8600811, Japan.
[9]Kuramochi Clinic Interpark, Utsunomiya, Tochigi 3210114, Japan.
[10]Human Genetics Laboratory, National Institute of Genetics, Mishima, Shizuoka 4118540, Japan.
[11]Department of Hematology and Oncology, Graduate School of Medicine, Kyoto University, Kyoto 6068507, Japan.
[12]Division of Infection and Immunity, UCL, London, UK.
[13]Africa Health Research Institute, Durban, South Africa.
[14]University of Cape Town, Cape Town 7701, South Africa.
[15] Max Planck Institute of Biochemistry, 82152 Martinsried, Germany.
[16]Wellcome-MRC Cambridge Stem Cell Institute, Cambridge, UK.
[17]Welcome Sanger Institute, Wellcome Genome Campus, Hinxton, Cambridge CB10 1SA, UK.

ACCELERATED ARTICLE PREVIEW

[18]European Molecular Biology Laboratory, European Bioinformatics Institute, EMBL-EBI, Wellcome Trust Genome Campus, Hinxton CB10 1SD, UK.
[19]Cambridge University Hospitals NHS Foundation Trust, Addenbrookes Hospital, Cambridge, UK.
[20]Cavendish Laboratory/Dept Physics, University of Cambridge, JJ Thomson Ave, Cambridge CB3 0HE, UK.
[21]Transplant and Regenerative Medicine Laboratory, Translational and Clinical Research Institute, Faculty of Medical Sciences, Newcastle University, Newcastle Upon Tyne, UK.
[22]Humabs Biomed SA, a subsidiary of Vir Biotechnology, 6500 Bellinzona, Switzerland
[23]Department of Virology, University of Cambridge, UK.
[24]Department of Physiology, Development and Neuroscience, University of Cambridge, Cambridge, UK.
[25]Howard Hughes Medical Institute, Seattle, WA 98195, USA.
[26]Max Planck Institute for Infection Biology, Berlin, Germany.
[27]NHS Blood and Transplant, Cambridge, UK.
[28]CREST, Japan Science and Technology Agency, Saitama 3220012, Japan.
[44]These authors contributed equally: Bo Meng, Adam Abdullahi, Isabella A.T.M Ferreira, Niluka Goonawardane, Akatsuki Saito, Izumi Kimura, Daichi Yamasoba.

*A list of authors and their affiliations appears at the end of the paper.

†e-mail: rkg20@cam.ac.uk; keisato@g.ecc.u-tokyo.ac.jp

ACCELERATED ARTICLE PREVIEW

The SARS-CoV-2 Omicron BA.1 variant emerged in 2021[1] and bears multiple spike mutations[2]. Here we show that Omicron spike has higher affinity for ACE2 compared to Delta as well as a marked change of antigenicity conferring significant evasion of therapeutic monoclonal and vaccine-elicited polyclonal neutralising antibodies after two doses. mRNA vaccination as a third vaccine dose rescues and broadens neutralisation. Importantly, antiviral drugs remdesivir and molnupiravir retain efficacy against Omicron BA.1. Replication was similar for Omicron and Delta virus isolates in human nasal epithelial cultures. However, in lower airway organoids, lung cells and gut cells, Omicron demonstrated lower replication. Omicron spike protein was less efficiently cleaved compared to Delta. Replication differences mapped to entry efficiency using spike pseudotyped virus (PV) assays. The defect for Omicron PV to enter specific cell types effectively correlated with higher cellular RNA expression of TMPRSS2, and knock down of TMPRSS2 impacted Delta entry to a greater extent than Omicron. Furthermore, drug inhibitors targeting specific entry pathways[3] demonstrated that the

Omicron spike inefficiently utilises the cellular protease TMPRSS2 that promotes cell entry via plasma membrane fusion, with greater dependency on cell entry via the endocytic pathway. Consistent with suboptimal S1/S2 cleavage and inability to utilise TMPRSS2, syncytium formation by the Omicron spike was markedly impaired compared to the Delta spike. Omicron's less efficient spike cleavage at S1/S2 is associated with shift in cellular tropism away from TMPRSS2 expressing cells, with implications for altered pathogenesis.

The Omicron variant, first detected in South Africa[1], carries over 30 mutations in its spike protein and has now spread internationally at ferocious pace. More than 20 substitutions exist on the N-terminal domain (NTD) and receptor binding domain (RBD). The Omicron variant also harbours six unique mutations in S2 (N764K, D796Y, N856K, Q954H, N969K, L981F) that were not previously detected in other variants of concern (VoC). Alpha and Delta variant spike proteins were previously shown to confer more efficient cell-cell fusion kinetics compared to Wuhan-1[4,5] due to mutations in the furin cleavage site region that increase S1/S2 cleavage, and syncytia formation previously associated with pathogenesis[6]. Omicron has three mutations in this region (P681H, H655Y and N679K) and was initially predicted to be highly infectious[7] and pathogenic. Indeed, the Omicron variant has been associated with very rapid increases in case numbers and recent data demonstrate significant re-infection and vaccine 'breakthrough', likely due to evasion of neutralising antibody responses[8,9]. Somewhat paradoxically however, recent findings suggest reduced severity in Omicron infections compared to Delta[10].

Here we explore biological properties of Omicron, and focus on spike mediated evasion of neutralising antibodies, increased ACE2 binding affinity, as well as a shift in tropism away from TMPRSS2 expressing cells and compromised ability to generate syncytia.

Omicron spike binding affinity to ACE2

The Omicron variant has 15 amino acid mutations in the RBD (Supplementary Figure 1 and 2). To understand the impact of these substitutions on receptor engagement, we determined the kinetics and affinity of monomeric human ACE2 binding to immobilized Omicron,

ACCELERATED ARTICLE PREVIEW

Wuhan-Hu-1 and Delta RBDs using biolayer interferometry (BLI). We observed that the Omicron RBD has a ~3-fold enhanced binding affinity for ACE2 relative to the Wuhan-Hu-1 and Delta RBDs (Table 1, Supplementary Figure 2), in line with previous findings[11-14].As previously observed for the Alpha RBD, which only harbors the N501Y mutation[15], the modulation of binding is mediated by changes in ACE2 binding off rates. Although the K417N mutation is known to dampen ACE2 engagement[15,16], a recently determined crystal structure of ACE2-bound Omicron RBD revealed that Q493R and Q498R introduce additional electrostatic interactions with ACE2 residues E35 and D38, respectively[16], whereas S477N enables hydrogen-bonding with ACE2 S19 (Supplementary Figure 2). Collectively, these mutations strengthen ACE2 binding, relative to the ancestral isolate. We extended this binding analysis to a cell based model using cells transfected with full-length spike, followed by ACE2 antibody titration; we observed significantly higher ACE2 binding for Omicron spike as compared to both Wuhan-1 and Delta variant spikes (Supplementary Figure 2). This enhanced binding could be a factor in the enhanced transmissibility of Omicron relative to previous variants.

Omicron sensitivity to therapeutics

Omicron was predicted to have broad resistance to neutralising antibodies based on mutations in class I-IV antigenic regions in the RBD[17]. Current standard of care antiviral treatment for moderate to severe COVID-19 includes use of the monoclonal antibody combination REGN 10933 and 10897. K417N, E484A, S477N, and Q493R preclude REGN10933 binding whereas G446S clashes with REGN10987, consistent with the dampened binding to the Omicron RBD and S trimer and loss of neutralization previously descibed[12,16]. We next tested serial dilutions of component mAbs, both individually and in combination, against Delta and Omicron live viruses in tissue culture (Figure 1a). Whilst the Delta variant was effectively neutralised by casivirimab, imdevimab was only partially effective, consistent with previous data[4]. In combination, these mAbs were highly potent against Delta. However, there was complete loss of neutralising activity against Omicron by either mAb alone or in combination (Figure 1a). Given these results, we next tested direct acting antivirals remdesivir and the active metabolite of molnupiravir against live virus. We observed similar antiviral activity against Delta and Omicron using serial titrations of both compounds (Supplementary Figure 3).

Omicron and polyclonal antibodies

ACCELERATED ARTICLE PREVIEW

A critical question is whether vaccine elicited antibodies are able to neutralise Omicron. We synthesised codon optimised spike expression plasmids for Omicron and Delta spike proteins and generated PV particles by co-transfecting the spike expression plasmids with a lentiviral gag-pol expressing plasmid and a lentiviral transduction plasmid encoding the luciferase gene[18,19]. We obtained longitudinal serum samples from 40 individuals vaccinated with either BNT162b2 or ChAdOx-1 vaccines and performed serum titrations before mixing sera with our reporter PV particles. Participants had median age of around 70 years and prospective serum samples were taken as follows: one month after dose two, six months after dose two, and one month after dose three (**Extended Data Table 2**). We observed ≥ 10-fold loss of neutralisation against Omicron after the second dose compared to Delta (**Figure 1b, c, Extended Data Figure 4**). Indeed neutralisation of Omicron was not detectable for the majority of individuals who had received two doses of ChAdOx-1. We additionally also observed waning over time since second dose for both vaccines (**Figure 1b,c**). Both groups were boosted with BNT162b2 as a third dose, allowing us to compare the response to this boosting dose. Very substantial increases (> 10 fold) in neutralisation against both Omicron and Delta were observed for all variants following third dose vaccination, suggesting increased breadth of responses as well as titre.

To confirm loss of neutralising activity against Omicron after the second dose, we next used a live virus experimental system to compare Delta and Omicron variants against sera taken four weeks after the second dose of BNT162b2, and obtained similar results as obtained in the PV assay (**Extended Data Figure 5a**). These live viruses were also used to assess the neutralisation of the Omicron variant by sera derived from non-vaccinated individuals previously infected with the early Wuhan-1 virus, or the Delta variant. As expected, vaccine sera had significantly impaired activity against Omicron as compared to Delta (**Extended Data Figure 5a**). We also tested mRNA 1273 vaccine elicited sera which showed similar reduction in neutralisation to BNT162b2. Coronavac sera however showed little neutralisation against Delta and 0/9 participants had detectable neutralisation against Omicron. Sera from Delta infections appeared to have lower cross neutralisation as compared to those from the early pandemic period when Wuhan-1 D614G was dominant (**Extended Data Figure 5b**).

Omicron replication and spike cleavage

ACCELERATED ARTICLE PREVIEW

We infected primary human nasal epithelial 3D cultures (hNEC) with an air liquid interface (**Figure 2a,b**). Infection with live SARS-CoV-2 Omicron or Delta was conducted at the apical surface with equal amounts of input virus and virus collected from the apical surface at 24 and 48 hours, with quantification of virus by E gene qPCR and TCID50. We observed similar replication kinetics for Omicron and Delta in the hNEC (**Figure 2b**). We next infected Calu-3 lung cells (known to express endogenous TMPRSS2) with live isolates, and observed significantly greater viral replication for Delta than Omicon (**Figure 2c**), manifesting as early as 24 hours post infection. We also infected Caco2, a colon cancer cell line (known to express high levels of endogenous TMPRSS2[20]), and, as for Calu-3, found one log greater Delta RNA and higher infectious virus (TCID50) in supernatants than was observed for Omicron. Finally we tested a cell line, HeLa, overexpressing ACE2 and TMPRSS2 with similar results as for Calu-3 and CaCo-2 cells.

We next sought to examine the possibility that the impaired replication in some cells may be related to differential spike incorporation and/or cleavage. For example Delta, known to have higher replication, is associated with a highly cleaved spike protein[4]. We tested purified virions from two independent Omicron isolate infections. We observed broadly similar amounts of Omicron and Delta spike incorporation into virions generated in VeroE6 ACE2/TMPRSS2 cells (**Figure 2f**). There was, however, reduced cleavage in whole Omicron virions compared to Delta as evidenced by the ratio of full length spike to S1 and S2; the Omicron spike was inefficiently cleaved in virions compared to Delta (**Figure 2f**). However, a more dramatically reduced Omicron spike cleavage relative to Delta was observed in cell lysates (**Figure 2g**).

Given lower intracellular S1/S2 cleavage for Omicron versus Delta spike proteins, confocal microscopy was used to explore whether cleavage efficiency was related to differences in sub cellular localisation. We analysed the distribution of Spike in cells infected with Omicron and Delta SARS-COV-2 live virus isolates (**Figure 2h-j**); no clear differences were observed between the variants in distance from the nucleus or co-localisation with a Golgi marker, indicating the subcellular localisation between Delta and Omicron is similar.

Omicron entry impaired in TMPRSS2+ cells

SARS-CoV-2 spike is a major determinant of viral infectivity and mediates cell entry via interaction with ACE2[3,11] and either TMPRSS2[3] at the plasma membrane or cathepsins in

ACCELERATED ARTICLE PREVIEW

endosomes. The plasma membrane route of entry, and indeed transmissibility and disease severity in animal models, is critically dependent on the polybasic cleavage site (PBCS) between S1 and S2[6,21] and cleavage of spike prior to virion release from producer cells; this contrasts with the endosomal entry route, which does not require spike cleavage in producer cells[3]. Plasma membrane fusion additionally allows the virus to avoid restriction factors in endosomes[7].

We tested spike mediated viral entry of WT Wuhan-1 D614G, Delta and Omicron spikes (**Figure 3a**) using the PV system. We first probed PV virions for spike protein and on western blotting noted reduced Omicron spike incorporation into virions compared to Delta (Extended Data Figure 6). We also noted that the Omicron spike was less cleaved than Delta as observed with live virus (**Extended Data Figure 6**). Of note cleavage of Omicron spike in cells was also lower compared to Delta and WT, again reminiscent of that in live virus.

Using normalised amounts of Delta and Omicron spike PV, we infected primary 3D lower airway organoids and gall bladder organoids [22,23] (**Figure 3a, Extended Data Figure 6**), in addition to Calu-3 lung cells. Mirroring the lower replication of Omicron relative to Delta in live virus assays, we observed impaired entry efficiency for Omicron spike in both organoid systems and the Calu-3 cells in comparison to Delta and Wuhan-1 D614G wild type. By contrast, in H1299 lung cancer epithelial cells, Hela-ACE2 (overexpressing ACE2), and 293T cells overexpressing ACE2 and deleted for TMPRSS2 (293T-A2ΔT2), we did not observe large differences in entry efficiency for Delta and Omicron (**Figure 3a**).

In order to further explore our PV entry and infection findings, we studied the expression of ACE2 and TMPRSS2 across our target cells by qPCR on RNA extracts from cell lysates (**Figure 3b**). We found greater TMPRSS2 mRNA in cells where Omicron PV entry was impaired relative to Delta: for example Calu-3 and Organoids were higher in TMPRSS2 compared to H1299, Hela-ACE2, and 293T-A2ΔT2. ACE2 levels were variable as expected, and did not appear to have a correlation with differences in infection between Omicron and Delta PV**.** We therefore hypothesised that the Omicron PV was disadvantaged relative to Delta in TMPRSS2-expressing cells.

To experimentally demonstrate differential usage of TMPRSS2 as a cofactor for virus entry by Omicron, we directly compared viral entry efficiency between 293T-A2ΔT2 and 293T-

ACCELERATED ARTICLE PREVIEW

A2T2 cells; enhanced infectivity was observed from both WT and Delta when TMPRSS2 was overexpressed, suggesting TMPRSS2 is additionally required for their optimal virus entry. In contrast, no difference was observed from Omicron PV indicating Omicron is inefficient in utilising TMPRSS2 for its entry (**Figure 3c**). We hypothesised that the modest degree of TMPRSS2 dependent enhancement (3.4x) for Delta and a complete lack of enhancement for Omicron over a single infection round might relate to the overexpression of ACE2 in this system. To explore this possibility we tested standard 293T cells expressing low endogenous levels of ACE2 and those transduced to overexpress TMPRSS2 (293T-T2). Indeed we observed a much greater increase in infection for Delta (34x) under T2 overexpression conditions and a smaller increase (6x) for Omicron in the presence of overexpressed TMPRSS2 (**Figure 3d).** Together these data support a reduced contribution of TMPRSS2 cofactor usage by Omicron spike, with modulation of the effect size by ACE2 expression levels. Given previous work on relationship between S1/S2 cleavage in producer cells and TMPRSS2 dependence[24,25], the most likely explanation for altered TMPRSS2 usage is the suboptimal S1/S2 cleavage in Omicron leading to inefficient S2' processing and fusion peptide exposure.

A change in use of TMPRSS2 for entry would be predicted to alter the entry pathway (**Figure 3e)**. To test the hypothesis of a change of entry route preference by Omicron spike away, we used inhibitors of proteases specific to either the endocytic pathway (E64D blockade of cathepsins), or the plasma membrane pathway (camostat blockade of TMPRSS2). We reasoned that if indeed Omicron has become more dependent on the endocytic cell entry route it should be more sensitive to cathepsin inhibition. We infected A549 cells overexpressing ACE2 and TMPRSS2 (A549-A2T2) cells in the presence of serial dilutions of E64D or camostat; indeed E64D had a greater effect on cell entry by Omicron PV versus Delta PV and conversely camostat had a greater effect on Delta PV entry (**Figure 3f**). We then performed this experiment with live virus isolates, using an indicator lung cell line (A549-A2T2), with a similar, albeit less dramatic, result as shown for PV (**Figure 3g**). These drug data in both live virus and PV systems further support the shift in tropism away from TMPRSS2 expressing cells.

Having established that TMPRSS2 modulates entry mediated by Delta to a greater extent than for Omicron BA.1 spike, we sought to understand the distribution of TMPRSS2 and ACE2 expression in human respiratory cells. We used single-nuclei RNA-seq data from 5

ACCELERATED ARTICLE PREVIEW

locations in the human lung[26]. The comparison revealed higher expression of TMPRSS2 in the alveolar AT1 and AT2 pneumocytes, and in general lower expression in the trachea (upper airway, **Extended Data Figure 7).** ACE2 expression was generally lower overall, but appeared higher in AT1 and AT2 cells as compared to other cell types, and also in club cells[27]. We experimentally extended these findings by performing qPCR on human lung tissues samples[28], showing higher mRNA expression of TMPRSS2 in lung parenchyma (alveolar) tissue compared to upper airway bronchial tissues and a trend towards ACE2 being higher in the upper airway tissue (**Figure 3h**).

Impaired cell-cell fusion by Omicron S

The ability of viral membrane glycoproteins to induce cell-cell fusion and syncytium formation is well established[29-31], providing an additional route for SARS-CoV-2 dissemination that may facilitate evasion of neutralising antibodies. The role of syncytium formation in viral replication and pathogenesis of severe COVID-19 has been reported and may be a druggable process to treat COVID-19 pathology[32,33]. SARS-CoV-2 mediated cell-cell fusion requires the polybasic cleavage site and spike cleavage at S1/2, and the process is known to be accelerated by the presence of TMPRSS2[29].

Mutations at P681 in the PBCS have been observed in multiple SARS-CoV-2 lineages, most notably in the B.1.1.7 Alpha variant[5] and the Delta/Kappa variants from the B.1.617 lineage[4,34]. We previously showed that spikes of these variants, all bearing P681 mutations, had significantly higher fusogenic potential than a D614G Wuhan-1 spike [4,35]. Omicron bears P681H, in addition to 679 and 655 mutations (**Supplementary Figure 6a**).

Given the requirement of TMPRSS2 for optimal cell-cell fusion, we hypothesised that Omicron may be impaired in mediating this process. We used a split GFP system[36] to monitor cell-cell fusion in real time (**Figure 4a**). As a control to show spike cleavage is needed for fusion in our assay system, we titrated CMK (a furin inhibitor) into donor cell media prior to transfection with spike expressing plasmids , observing dose dependent inhibition of fusion (Extended Data Figure 8). As a further control to demonstrate the need for ACE2 engagement by expressed spike, we tested the ability of convalescent serum containing neutralising antibodies to block cell-cell fusion. Indeed serum blocked syncytia formation in a dose dependent manner (Extended Data Figure 8).

ACCELERATED ARTICLE PREVIEW

We performed flow cytometry to verify that spike was expressed at the cell surface (Figure 4b). We proceeded to transfect spike bearing plasmids into 293T cells expressing GFP1-10 and Vero E6 cells stably expressing the GFP-11, so that the GFP signal could be detected upon cell-cell fusion and measured over time. (**Figure 4c,d**). We observed increased fusion for Delta as compared to D614G Wuhan-1 spike (**Figure 4d**). The Omicron spike however resulted in very poor fusion (**Figure 4d)**.

We predicted that poor fusion would impair cell-cell spread of Omicron, and analysed infection focus size using live virus infection of H1299 cells, in which we have shown similar entry efficiency for Omicron and Delta spike PV, see Figure 3. Infection foci in spreading virus infections occurs because of localized (cell-to-cell) infection, likely facilitated by syncitium formation. The infection was followed by overlay of semi-solid media (carboxymethylcellulose) to inhibit cell-free infection, thereby favouring cell-cell infection. Infected cells were stained with an anti-S antibody, and local spread characterised by staining of foci visible to the naked eye (**Figure 4e**). Omicron infection resulted in slightly higher numbers of foci (**Figure 4e-g**), but each infection focus was substantially smaller in size relative to those formed by the Delta (**Figure 4e**). For a more detailed view of the foci, we imaged at a higher magnification with a microscope objective, and used cells imaged 2 hours post-ancestral virus infection, when relatively little viral transmission is expected to be completed, as an approximate measure of the size of a single cell (**Extended Data Figure 8**). We compared this to cells infected for 18 hours by Omicron or Delta isolates. Size of foci at 2 hours post-ancestral virus infection was $1.2x10^3$ micron^2 (95% CI 0.9-$1.5x10^3$). The size of Omicron foci was $1.5x10^3$ micron^2 (95% CI 1.4-$1.5x10^3$), and in contrast, Delta focus size was $3.4x10^3$ micron^2 (95% CI 3.1-$3.7x10^3$), 2.3-fold higher than Omicron (**Extended Data Figure 8**). Together, these results show that localized cell-cell infection of Omicron is reduced relative to Delta, consistent with attenuated cell-cell fusion.

Discussion

Here we have explored biological properties of Omicron from the perspectives of spike mediated immune evasion, ACE2 binding interactions, and cellular entry pathways that dictate tissue tropism. We have shown firstly that the Omicron spike confers significant evasion of vaccine elicited neutralising antibodies that is more dramatic for ChAdOx-1 versus BNT162b2 vaccine sera. In longitudinally sampled participants, second dose waning was mitigated by third dose mRNA vaccination that also increased and broadened

ACCELERATED ARTICLE PREVIEW

neutralisation of Omicron in the short term. This observation is critical for informing third dose vaccination efforts worldwide. Critically, ChAdOx-1 is widely used in low income settings where third doses with mRNA not widely available, and Omicron may contribute to higher infection rates and severe disease in such settings unless third doses can be implemented. Of further concern for low income countries was the absence of any neutralising activity to Omicron in sera after two doses of Coronavac in all nine participants, in addition to poor Delta neutralisation.

In terms of implications for treatment options for moderate to severe clinical disease, we show high level loss of *in vitro* activity for the widely used mAb combination therapy REGN2 against Omicron, but no significant loss of activity of the polymerase inhibitors remdesivir and molnupiravir against live virus. The mAb sotrovimab has also been reported to retain significant *in vitro* activity against Omicron[12,37].

Despite the presence of three mutations that are individually predicted to favour spike S1/S2 cleavage, the observed cleavage of spike in cells infected with live virus was lower compared to Delta and WT Wuhan-1 D614G. Similarly, live Omicron virions had a lower proportion of cleaved spike than Delta. Cleavage deficiency was also evident in PV particles. We previously noted that the proportion of cleaved spike was lower within cells as compared to virions[4], suggesting that incorporation of spike into virions produced in the ERGIC (ER-Golgi intermediate compartment) may favour cleaved spike over full length spike, or be cleaved as virions are secreted through exocytic pathways[38].

Live Omicron virus showed a significant replication defect as compared to Delta cell culture systems where TMPRSS2 was present. Omicron spike was also associated with decreased entry relative to both WT and Delta spikes in target lower airway organoids, gallbladder organoids or Calu-3 lung cells expressing TMPRSS2, but displayed no difference in cells where TMPRSS2 expression is low, for example H1299, Hela-ACE2 and 293T-A2. We proceeded to directly compare entry in ACE2 overexpressing cells where TMPRSS2 was either knocked down or overexpressed and showed that Omicron entry was not impacted by variations in TMPRSS2 expression, in stark contrast to WT and Delta spike PV entry. When ACE2 was not overexpressed, we importantly observed a large increase for Delta PV entry with TMPRSS2 availability, and a much smaller increase in entry for Omicron. These data suggest that TMPRSS2 cofactor usage may be impacted by ACE2 levels. The hypothesis that

ACCELERATED ARTICLE PREVIEW

Omicron spike has altered its preference to the cathepsin dependent endosomal route of entry (TMPRSS2-independent) was borne out by inhibitor experiments against cathepsin and TMPRSS2 in both PV and live virus isolates.

TMPRSS2 is a member of the TTSP family (TTSP – Type II Transmembran Serine Protease). This family comprises 17 members with diverse physiological functions. These proteins require activation and remain associated with membranes, and TMPRSS2 in particular can undergo autocatalytic activation[39], though its role in human physiology is unclear. TMPRSS2 has been shown to be a cofactor for SARS-CoV-1 and MERS as well as SARS-CoV-2[3,40]. Importantly, TMPRSS2-dependence correlates with efficient cleavage at the PBCS between S1/S2[24,25], with removal of the furin cleavage site in SARS-CoV-2 reducing TMPRSS2 dependence. By contrast, experiments where a furin cleavage site was introduced into SARS-CoV-1 demonstrated greater TMPRSS2 dependence.

Omicron presents an interesting parallel with SARS-CoV-1, which is not cleaved in the producer cell due to lack of the PBCS, but rather on the target cell surface by TMPRSS2 or by cathepsins in endosomes. SARS-CoV-1 is able to infect cells (i) via TMPRSS2 (and therefore syncytia can be induced[31]), or (ii) by endocytosis[3,25]. SARS-CoV-2 Omicron variant appears to also favour endocytosis through reduced cleavage efficiency of spike impairing TMPRSS2 mediated entry. Indeed, the accumulated mutations in omicron include multiple additional basic amino acids leading to an increase in the overall charge of the S protein. This change may make S more sensitive to low-pH induced conformational changes, and be an adaptation that facilitates use of the low-pH endosomal entry route, and/or to entry in the lower pH environment in the upper airway. Furthermore, our analysis of scRNA-seq datasets and direct qPCR measurements on human respiratory tissue samples suggest that lung cells have higher TMPRSS2 mRNA as compared to cells found in the upper airway. Indeed recent data indicate lower virus burden in deep lung tissue and reduced pathogenicity in Omicron versus Delta infections using Syrian hamster models[41].

As expected from suboptimal cleavage of spike in producer cells, and the known link between efficient spike cleavage and ability to use TMPRSS2 for cell entry / cell-cell fusion, we observed low fusogenic potential of the Omicron spike. This phenomenon could translate to impaired cell-cell spread, and indeed we observed smaller plaque sizes for Omicron compared to Delta in a system where cell free infection was limited by semi-solid medium.

ACCELERATED ARTICLE PREVIEW

The smaller focus size for Omicron could be attributable to failure to induce syncytia, without compromised entry efficiency given similar foci number observed. The semi solid media has prevented cell free infection and therefore our measurement should primarily reflect infection spread over a limited time period via syncytia formation. However, the smaller foci could have differing implications in vivo. First, there may be decreased virus production due to less cell death, therefore favouring Omicron over Delta. Alternatively, syncytia along with cell survival with larger infection foci may increase spread, thereby favouring Delta. The difference in outcome from syncytia is likely to be cell and tissue dependent and we caution against extrapolation of these *in vitro* infection data to viral loads in the respiratory tract.

Our data showing tropism differences for Omicron in organoid systems and human nasal epithelial cultures are limited by the fact that they are in vitro systems, albeit using primary human tissue. It should also be noted that levels of TMPRRS2 may impact ACE2, particularly as TMPRSS2 has been implicated in ACE2 cleavage[42] and our effect sizes were impacted by ACE2 expression. Finally, E64D may inhibit viral protease in addition to host cellular cathepsins, and this may have impacted the strength of the observed phenotype.

In summary, Omicron has gained immune evasion properties whilst compromising cell entry in TMPRSS2 expressing cells such as those in alveoli, as well as compromising syncytia formation: a combination of traits consistent with reduced pathogenicity *in vivo*. Crucially, experience with Omicron has demonstrated that predictions regarding replication and tropism based on sequence alone can be misleading, and detailed molecular understanding of the tropism change is vital as variants continue to emerge.

Online content Any methods, additional references, Nature Research reporting summaries, source data, extended data, supplementary information, acknowledgements, peer review information; details of author contributions and competing interests; and statements of data and code availability are available at [Article DOI].

Received 21 December 2021; accepted 26 January 2022

1 Viana, R. *et al.* Rapid epidemic expansion of the SARS-CoV-2 Omicron variant in southern Africa. *Nature*, doi:10.1038/s41586-022-04411-y (2022).
2 Cele, S. *et al.* Omicron extensively but incompletely escapes Pfizer BNT162b2 neutralization. *Nature*, doi:10.1038/s41586-021-04387-1 (2021).

ACCELERATED ARTICLE PREVIEW

3 Hoffmann, M. *et al.* SARS-CoV-2 Cell Entry Depends on ACE2 and TMPRSS2 and Is Blocked by a Clinically Proven Protease Inhibitor. *Cell* **181**, 271-280 e278, doi:10.1016/j.cell.2020.02.052 (2020).
4 Mlcochova, P. *et al.* SARS-CoV-2 B.1.617.2 Delta variant replication and immune evasion. *Nature* **599**, 114-119, doi:10.1038/s41586-021-03944-y (2021).
5 Meng, B. *et al.* Recurrent emergence of SARS-CoV-2 spike deletion H69/V70 and its role in the Alpha variant B.1.1.7. *Cell reports* **35**, 109292, doi:10.1016/j.celrep.2021.109292 (2021).
6 Saito, A. *et al.* Enhanced fusogenicity and pathogenicity of SARS-CoV-2 Delta P681R mutation. *Nature*, doi:10.1038/s41586-021-04266-9 (2021).
7 Peacock, T. P. *et al.* The furin cleavage site in the SARS-CoV-2 spike protein is required for transmission in ferrets. *Nat Microbiol*, doi:10.1038/s41564-021-00908-w (2021).
8 Cele, S. *et al.* SARS-CoV-2 Omicron has extensive but incomplete escape of Pfizer BNT162b2 elicited neutralization and requires ACE2 for infection. *medRxiv*, 2021.2012.2008.21267417, doi:10.1101/2021.12.08.21267417 (2021).
9 Dejnirattisai, W. *et al.* Reduced neutralisation of SARS-COV-2 Omicron-B.1.1.529 variant by post-immunisation serum. *medRxiv*, 2021.2012.2010.21267534, doi:10.1101/2021.12.10.21267534 (2021).
10 Wolter, N. *et al.* Early assessment of the clinical severity of the SARS-CoV-2 Omicron variant in South Africa. *medRxiv*, 2021.2012.2021.21268116, doi:10.1101/2021.12.21.21268116 (2021).
11 Walls, A. C. *et al.* Structure, Function, and Antigenicity of the SARS-CoV-2 Spike Glycoprotein. *Cell* **181**, 281-292 e286, doi:10.1016/j.cell.2020.02.058 (2020).
12 Cameroni, E. *et al.* Broadly neutralizing antibodies overcome SARS-CoV-2 Omicron antigenic shift. *Nature*, doi:10.1038/s41586-021-04386-2 (2021).
13 Starr, T. N. *et al.* Deep Mutational Scanning of SARS-CoV-2 Receptor Binding Domain Reveals Constraints on Folding and ACE2 Binding. *Cell* **182**, 1295-1310 e1220, doi:10.1016/j.cell.2020.08.012 (2020).
14 McCallum, M. *et al.* Molecular basis of immune evasion by the Delta and Kappa SARS-CoV-2 variants. *Science* **374**, 1621-1626, doi:10.1126/science.abl8506 (2021).
15 Collier, D. A. *et al.* SARS-CoV-2 B.1.1.7 sensitivity to mRNA vaccine-elicited, convalescent and monoclonal antibodies. *Nature* **593**, 136-141, doi:10.1101/2021.01.19.21249840 (2021).
16 McCallum, M. *et al.* Structural basis of SARS-CoV-2 Omicron immune evasion and receptor engagement. *Science*, doi:DOI: 10.1126/science.abn8652 (2021).
17 Barnes, C. O. *et al.* SARS-CoV-2 neutralizing antibody structures inform therapeutic strategies. *Nature* **588**, 682-687, doi:10.1038/s41586-020-2852-1 (2020).
18 Naldini, L. *et al.* In vivo gene delivery and stable transduction of non-dividing cells by a lentiviral vector. *Science* **272**, 263-267 (1996).
19 Mlcochova, P. *et al.* Combined point of care nucleic acid and antibody testing for SARS-CoV-2 following emergence of D614G Spike Variant. *Cell Rep Med*, 100099, doi:10.1016/j.xcrm.2020.100099 (2020).
20 Pommerenke, C. *et al.* Identification of cell lines CL-14, CL-40 and CAL-51 as suitable models for SARS-CoV-2 infection studies. *PloS one* **16**, e0255622, doi:10.1371/journal.pone.0255622 (2021).

ACCELERATED ARTICLE PREVIEW

21 Peacock, T. P. *et al.* The furin cleavage site in the SARS-CoV-2 spike protein is required for transmission in ferrets. *Nat Microbiol* **6**, 899-909, doi:10.1038/s41564-021-00908-w (2021).
22 Youk, J. *et al.* Three-Dimensional Human Alveolar Stem Cell Culture Models Reveal Infection Response to SARS-CoV-2. *Cell Stem Cell* **27**, 905-919 e910, doi:10.1016/j.stem.2020.10.004 (2020).
23 Sachs, N. *et al.* Long-term expanding human airway organoids for disease modeling. *The EMBO journal* **38**, doi:10.15252/embj.2018100300 (2019).
24 Papa, G. *et al.* Furin cleavage of SARS-CoV-2 Spike promotes but is not essential for infection and cell-cell fusion. *PLoS pathogens* **17**, e1009246, doi:10.1371/journal.ppat.1009246 (2021).
25 Ou, T. *et al.* Hydroxychloroquine-mediated inhibition of SARS-CoV-2 entry is attenuated by TMPRSS2. *PLoS pathogens* **17**, e1009212, doi:10.1371/journal.ppat.1009212 (2021).
26 Madissoon, E. *et al.* A spatial multi-omics atlas of the human lung reveals a novel immune cell survival niche. *bioRxiv*, 2021.2011.2026.470108, doi:10.1101/2021.11.26.470108 (2021).
27 Salahudeen, A. A. *et al.* Progenitor identification and SARS-CoV-2 infection in human distal lung organoids. *Nature* **588**, 670-675, doi:10.1038/s41586-020-3014-1 (2020).
28 Brevini, T. *et al.* FXR inhibition reduces ACE2 expression, SARS-CoV-2 infection and may improve COVID-19 outcome. *bioRxiv*, 2021.2006.2006.446781, doi:10.1101/2021.06.06.446781 (2021).
29 Buchrieser, J. *et al.* Syncytia formation by SARS-CoV-2-infected cells. *The EMBO journal* **40**, e107405, doi:10.15252/embj.2020107405 (2021).
30 Cattin-Ortolá, J. *et al.* Sequences in the cytoplasmic tail of SARS-CoV-2 Spike facilitate expression at the cell surface and syncytia formation. *bioRxiv*, 2020.2010.2012.335562, doi:10.1101/2020.10.12.335562 (2021).
31 Li, W. *et al.* Angiotensin-converting enzyme 2 is a functional receptor for the SARS coronavirus. *Nature* **426**, 450-454, doi:10.1038/nature02145 (2003).
32 Braga, L. *et al.* Drugs that inhibit TMEM16 proteins block SARS-CoV-2 Spike-induced syncytia. *Nature*, doi:10.1038/s41586-021-03491-6 (2021).
33 Bussani, R. *et al.* Persistence of viral RNA, pneumocyte syncytia and thrombosis are hallmarks of advanced COVID-19 pathology. *EBioMedicine* **61**, 103104, doi:10.1016/j.ebiom.2020.103104 (2020).
34 Ferreira, I. *et al.* SARS-CoV-2 B.1.617 Mutations L452R and E484Q Are Not Synergistic for Antibody Evasion. *The Journal of infectious diseases* **224**, 989-994, doi:10.1093/infdis/jiab368 (2021).
35 Meng, B. *et al.* Recurrent emergence and transmission of a SARS-CoV-2 spike deletion H69/V70 and role in Alpha Variant B.1.1.7. *Cell reports*, doi:https://doi.org/10.1016/j.celrep.2021.109292 (2021).
36 Cabantous, S., Terwilliger, T. C. & Waldo, G. S. Protein tagging and detection with engineered self-assembling fragments of green fluorescent protein. *Nature biotechnology* **23**, 102-107, doi:10.1038/nbt1044 (2005).
37 Cathcart, A. L. *et al.* The dual function monoclonal antibodies VIR-7831 and VIR-7832 demonstrate potent in vitro and in vivo activity against SARS-CoV-2. *bioRxiv*, 2021.2003.2009.434607, doi:10.1101/2021.03.09.434607 (2021).

ACCELERATED ARTICLE PREVIEW

38 V'Kovski, P., Kratzel, A., Steiner, S., Stalder, H. & Thiel, V. Coronavirus biology and replication: implications for SARS-CoV-2. *Nat Rev Microbiol* **19**, 155-170, doi:10.1038/s41579-020-00468-6 (2021).
39 Bugge, T. H., Antalis, T. M. & Wu, Q. Type II transmembrane serine proteases. *The Journal of biological chemistry* **284**, 23177-23181, doi:10.1074/jbc.R109.021006 (2009).
40 Park, J. E. *et al.* Proteolytic processing of Middle East respiratory syndrome coronavirus spikes expands virus tropism. *Proceedings of the National Academy of Sciences of the United States of America* **113**, 12262-12267, doi:10.1073/pnas.1608147113 (2016).
41 collaboration, J. P. Attenuated replication and pathogenesis of SARS-CoV-2 B.1.1.529 Omicron. *Research Square* (2021).
42 Heurich, A. *et al.* TMPRSS2 and ADAM17 cleave ACE2 differentially and only proteolysis by TMPRSS2 augments entry driven by the severe acute respiratory syndrome coronavirus spike protein. *Journal of virology* **88**, 1293-1307, doi:10.1128/JVI.02202-13 (2014).

Publisher's note: Springer Nature remains neutral with regard to jurisdictional claims in published maps and institutional affiliations.

Methods

Serum and tissue samples and ethical approval

Ethical approval for study of vaccine elicited antibodies in sera from vaccinees was obtained from the East of England – Cambridge Central Research Ethics Committee Cambridge (REC ref: 17/EE/0025). Participants provided informed consent. The samples of human upper and lower airways were obtained from the lungs of a multiorgan donor whose lungs were deemed unsuitable for clinical transplantation and after their next of kin consented to their use in research. The studies using human donor lungs tissue were approved by National Research Ethics Committee (NREC) 16/NE/0230.

The virus isolation procedures in this study were approved by the Institutional Review Board of National Institute for Infectious Diseases (approval ID: 1178) and Tokyo Metropolitan Institute of Public Health (approval ID: 3KenKenKen-466) according to the Declaration of Helsinki 2013. All protocols involving specimens from human subjects recruited at Kyoto University, Kuramochi Clinic Interpark and Universidad San Francisco de Quito were reviewed and approved by the Institutional Review Boards of Kyoto University (approval ID: G0697), Kuramochi Clinic Interpark (approval ID: G2021-004) and Universidad San

ACCELERATED ARTICLE PREVIEW

Francisco de Quito (approval ID: CEISH P2020-022IN), and the Ecuadorian Ministry of Health (approval IDs: MSP-CGDES-2020-0121-O and MSP-CGDES-061-2020). The export of sera from Ecuador to Japan was approved by ARCSA ID: ARCSA-ARCSA-CGTC-DTRSNSOYA-2021-1626-M. All human subjects provided written informed consent. All protocols for the use of human specimens were reviewed and approved by the Institutional Review Boards of The Institute of Medical Science, The University of Tokyo (approval ID: 2021-1-0416), Kumamoto University (approval IDs: 2066 and 2074), University of Miyazaki (approval ID: O-1021)

Omicron spike model showing surface mutations with annotation

Spike genomes for the original Wuhan strain, and Omicron VOC were obtained from GISAID EpiCoV database accessed on 30th November 2021. A consensus Spike genome was created from all complete and high coverage genomes, excluding all sequences with >5% Ns using Geneious Prime v2022. The consensus genome was translated to poly-proteins and the Spike gene was aligned to the original Wuhan strain using mafft v7.490[43] with the --globalpair --maxiterate 1000 flags.

3D structural models of the spike homotrimer protein complex were alternatively also generated using Alphafold v2.1.1[44]. In its validation at the 14th edition of the Critical Assessment of protein Structure Prediction (CASP14) the predictions generated were demonstrated to be comparative to experimental structures. When a close homolog structure is available to Alphafold the predictions it generates for those positions are within typical experimental error. Required databases were downloaded on 02/12/2021. The program was run with the parameters --max_template_date=2021-12-01 --model_preset=monomer --db_preset=full_dbs --is_prokaryote_list=false. Protein structures were visualised in ChimeraX v1.3[45]. As predicted structures for the whole spike protein include poorly resolved chains at the terminal ends, these residues were identified by overlaying structures on PDB entry 6ZP2, then selected and removed from PDB files using the delete atoms/bonds action. Two further monomers were overlayed on 6zp2 to generate a homotrimer structure. Mutated residues were then coloured in red and labelled manually with respect to the Wuhan strain.

Spike model comparing Delta and Omicron

The SARS-CoV-2 Delta (B.1.617.2) and Omicron (B.1.529) models in Extended Data Figure 1a were generated using the cryo-EM structure PDB# 7A94 as a reference. The experimental

ACCELERATED ARTICLE PREVIEW

structure has been resolved in open conformational state with one RBD in "up" conformation bound to ACE2. To generate the complete structure, the missing loop regions in the structure [71–75, 625–632, 677–688, 828–852, and 941–943] were modelled using Modeller plug-in[2]. The hACE2 structure in the template also had six residues missing patches that were added by taking PDB ID 1R42 as a reference[3]. The top model was selected on the basis of the zDOPE score and least RMSD with the reference structure. To create variant models, mutations were induced using the Dunbrack 2010 backbone-dependent rotamer library in Chimera[4]. Further processing of steps involving minimisation and peptide bond building (after deletions for B.1.617.2 and B.1.529 spike) were performed using the Gromacs. The resultant Delta and Omicron modelled complex have 3988 and 3994 residues, respectively with spike trimer consisting of three chains (14-1146) residues. The structural superimposition of Delta and Omicron spike model with cryo-EM structure displayed an overall RMSD of 0.66 Å and 0.87 Å, respectively. All the molecular images were rendered using ChimeraX[5].

Biolayer Interferometry

Assays were performed on an Octet Red (ForteBio) instrument at 30°C with shaking at 1,000 RPM. Streptavidin (SA) biosensors were hydrated in water for 10 min prior to a 1 min incubation in undiluted 10X kinetics buffer. SARS-CoV-2 Wuhan, Delta, or Omicron RBDs were loaded at 2.5 μg/mL in 10X Kinetics Buffer for 100-150 s prior to baseline equilibration for 120 s in 10X kinetics buffer. Human ACE2 association with Wuhan, Delta, and Omicron RBDs was assessed in 10X kinetics buffer at various concentrations in a three-fold dilution series from 333.3 to 4.1 nM and carried out for 300 s prior to dissociation for 300 s. The data were normalized to the baseline and fitting was performed using a 1:1 binding model and the ForteBio data analysis software. Kinetics values (K_D, k_{on}, k_{off}) were determined with a global fit applied to all data.

The SARS-CoV-2-RBD-Avi constructs were synthesized by GenScript into pcDNA3.1- with an N-terminal mu-phosphatase signal peptide and a C-terminal octa-histidine tag, flexible linker, and avi tag (GHHHHHHHHGGSSGLNDIFEAQKIEWHE). The boundaries of the construct are N-328RFPN331 and 528KKST531-C[46,47]. The human angiotensin-converting enzyme ectodomain (hACE2) consists of residues 1–614 fused to a C-terminal octa-histidine

ACCELERATED ARTICLE PREVIEW

tag[48]. Proteins were produced in Expi293F Cells (ThermoFisher Scientific) grown in suspension using Expi293 Expression Medium (ThermoFisher Scientific) at 37°C in a humidified 8% CO_2 incubator rotating at 130 rpm. Cells grown to a density of 3 million cells per mL were transfected using the ExpiFectamine 293 Transfection Kit (ThermoFisher Scientific) and cultivated for 4 days. Proteins were purified from clarified supernatants using a nickel HisTrap HP affinity column (Cytiva) and washed with ten column volumes of 20 mM imidazole, 25 mM sodium phosphate pH 8.0, and 300 mM NaCl before elution on a gradient to 500 mM imidazole. Proteins were buffer exchanged into 20 mM sodium phosphate pH 8 and 100 mM NaCl and concentrated using centrifugal filters (Amicon Ultra) before being flash frozen.

Flow Cytometry analysis of Spike protein surface expression

ExpiCHO cells were seeded into 50 ml Mini Bioreactor Centrifuge Tube (Corning) at 6 x 10^6 cells/ml in 5 ml ExpiCHO Expression medium (Life technology). Plasmids encoding SARS-CoV-2 Wuhan, Alpha (B.1.1.7), Delta (B.1.617.2) or Omicron (B.1.1.529) Spike protein (5 mg) were diluted in OptiPRO SFM (Life Technology) and mixed with Expifectamine CHO Reagent (Life Technology). After 1 min incubation at room temperature, transfection mixes were added to cell suspensions. Next, cells were incubated at 37°C 8% CO_2 with an orbital shaking speed of 120 rpm for the following 48 hours.

Transiently transfected cells were harvested and washed with PBS, 1% BSA, 2 mM EDTA. Cells were counted, dispensed into round-bottom 96 well plates (Corning) and incubated with human IgG Fc-conjugated ACE2 serial dilutions (concentration range: 30'000 – 0.17 ng/ml) for 45 min at 4°C. After two washes, Alexa Fluor647 Goat Anti-Human IgG secondary Ab (1.5 mg/ml) (Jackson Immunoresearch) was added to the cells, which were then incubated for 30 min at 4°C in the dark. Cells were washed twice and resuspended in wash buffer for data acquisition at ZE5 cytometer (Biorad). To assess Spike protein expression level, an aliquot of each transfectant cell line was stained with 10 mg/ml of S2P6 antibody[49] for 45 min at 4°C.

Analysis of single-nuclei and single-cell RNA sequencing datasets.

For the tissue data[50], only single-nuclei RNA-seq were selected. Scanpy 1.7.1 was used to process the data. ACE2 and TMPRSS2 expression was plotted with violin plot function in scanpy.

Cells and cell culture

ACCELERATED ARTICLE PREVIEW

Caco-2 Caco-2 cells transduced with BVDV NPro (Caco-NPro) were cultured in Dulbecco's modified Eagle's medium (DMEM) supplemented with 10% FCS, non-essential amino acid (NEAA), glutamine and 100 U penicillin ml^{-1} and 100 µg streptomycin ml^{-1} at 37 °C with 5% CO_2. HOS-ACE2/TMPRSS2 cells (HOS cells stably expressing human ACE2 and TMPRESS2)[51,52] were maintained in Dulbecco's modified Eagle's medium (high glucose) (Wako, Cat# 044-29765) containing 10% foetal bovine serum (FBS) and 1% PS. VeroE6/TMPRSS2 cells [an African green monkey (*Chlorocebus sabaeus*) kidney cell line; JCRB1819][53] were maintained in Dulbecco's modified Eagle's medium (low glucose) (Wako, Cat# 041-29775) containing 10% FBS, G418 (1 mg/ml; Nacalai Tesque, Cat# G8168-10ML) and 1% PS. Calu-3 (a human lung epithelial cell line; a gift from Paul Lehner, University of Cambridge or ATCC HTB-55) were maintained in Eagle's minimum essential medium (Sigma-Aldrich, Cat# M4655-500ML) containing 10% FBS and 1% PS.Vero E6 (ATCC-CRL1586), Vero-ACE2/TMPRSS2 (a gift from Emma Thomson were maintained in Dulbecco's modified Eagle's medium (low glucose) (Wako, Cat# 041-29775) containing 10% FBS, G418 (1 mg/ml; Nacalai Tesque, Cat# G8168-10ML) and 1% PS. Hela-ACE2 (a gift from James Voss), A549-ACE2/TMPRSS2 (a gift from Massimo Palmarini and HeLa-ACE2/TMPRSS2 were maintained in DMEM containing 10% FBS and 1% PS. 293T (CRL-3216), and its derivative cell lines including 293T-ACE2/TMPRSS2, 293T-ACE2ΔTMPRSS2, 293T-TMPRSS2, 293T-GFP11 have been described previously[54] and were kindly provided by Leo James, LMB. All the 293T cell lines as well as Vero-GFP1-10 (also a gift from Leo James, LMB) were maintained in DMEM with 10% FBS and 1% PS. H1299 cells (a gift from Simon Cook, Babraham Institute) were maintained in RPMI supplemented with 10% FCS and 1% PS. All cells were regularly tested and are mycoplasma free. Airway epithelial organoids and Gall bladder organoids were obtained and maintained as previously described[55,56]. **For airway organoids,** human distal lung parenchymal tissues were obtained from adult donors with no background lung pathologies from Papworth Hospital Research Tissue Bank (T02233). Airway organoids were cultured in 48-well plate were passaged every 2 weeks. For passaging, Matrigel was melted by incubation with dispase at 37°C for 30 min, followed by single cell dissociation by TrypLE (Gibco) at 37°C for 5 min. 5,000 cells were resuspended in fresh GFR-Matrigel, followed by plating in 48 well plates. Primary cholangiocyte organoids isolated from primary biliary tissue (intrahepatic ducts, common bile duct and gallbladder) and cultured using established methodology as previously reported[55].

ACCELERATED ARTICLE PREVIEW

Virus isolates

Lineages **B.1.1.617.2** (Delta, GISAID accession no EPI_ISL_1731019) and **B.1.1.529**[57] (Omicron UK isolate M21021166[58] – Gavin Screaton, Oxford University) were kindly received as part of the work conducted by G2P-UK National Virology Consortium (Barclay PI). Virus was propagated on Vero-ACE2-TMPRSS2 (VAT) cells for 3 days until cytopathic effect was observed. These viruses were sequence confirmed and were used for western blotting and Caco-3 gut experiments.

A second Omicron isolate from South Africa was obtained (GISAID EPI_ISL_7886688), and used specifically as a second isolate for western blotting of live virions and for focus size experiments. To isolate virus, ACE2-expressing H1299 cells were seeded at 4.5 × 105 cells in a 6 well plate well and incubated for 18–20 h. After one DPBS wash, the sub-confluent cell monolayer was inoculated with 500 µL universal transport medium diluted 1:1 with growth medium filtered through a 0.45-µm filter. Cells were incubated for 1 h. Wells were then filled with 3 mL complete growth medium. After 4 days of infection (completion of passage 1 (P1)), cells were trypsinized, centrifuged at 300 rcf for 3 min and resuspended in 4 mL growth medium. Then all infected cells were added to Vero E6 cells that had been seeded at 2 × 10^5 cells per mL, 20mL total, 18–20 h earlier in a T75 flask for cell-to-cell infection. The coculture of ACE2-expressing H1299-E3 and Vero E6 cells was incubated for 1 h and the flask was then filled with 20 mL of complete growth medium and incubated for 4 days. The viral supernatant (passage 2 (P2) stock) was used for experiments.P2 stock was sequenced and confirmed Omicron BA.1. The sequence was deposited in GISAID, with accession number: EPI_ISL_7886688.

A third Omicron isolate (BA.1 lineage, strain TY38-873; GISAID ID: EPI_ISL_7418017) with same mutational profile as other Omicron variant isolates and kindly provided by the National Institute for Infectious Diseases, Japan, was used for hNEC, Calu-3 and Hela-ACE2-TMPRSS2 infection experiments. Virus isolation was performed as previously described[53]. In brief, the saliva was inoculated into VeroE6/TMPRSS2 cells and cytopathic effect (CPE) was observed 4 days after inoculation. The supernatant was then harvested and stored at –80°C as an original virus (GISAID ID: EPI_ISL_7418017). After one more passage in VeroE6/TMPRSS2 cells, the following virus was additionally obtained from

ACCELERATED ARTICLE PREVIEW

National Institute of Infectious Diseases, Japan for hNEC experiments: Delta isolate (B.1.617.2 lineage, strain TKYTK1734; GISAID ID: EPI_ISL_2378732) [52]. Virus preparation and titration of virus isolates was performed as previously described[52,59]. To prepare the working virus stock, 100 µl of the seed virus was inoculated into VeroE6/TMPRSS2 cells (5×10^6 cells in a T-75 flask). Briefly, one hour after infection, the culture medium was replaced with culture media. At 3 days post-infection, the culture medium was harvested and centrifuged, and the supernatants were collected as the working virus stock. The titre of the prepared working virus was measured as the 50% tissue culture infectious dose ($TCID_{50}$). VeroE6/TMPRSS2 cells (in a 96-well plate. Serially diluted virus stocks were inoculated into the cells and incubated at 37°C for 4 days. The cells were observed under microscopy to judge the CPE appearance. The value of $TCID_{50}$/ml was calculated with the Reed–Muench method.

Sera Collection for live virus neutralisation experiments

Vaccine sera were collected from fourteen vaccinees four weeks after the second vaccination with BNT162b2 (Pfizer-BioNTech) (average age: 46, range: 38-55, 21% male). The sera obtained from seven vaccinees 2-3 weeks after the second vaccination with ChAdOx1 (Oxford-AstraZeneca) (average age: 46, range: 35-54, 71% male) were purchased from BioIVT.

Convalescent sera were collected from ten vaccine-naive individuals who had been infected with Delta variant (AY.29) (average age: 46, range: 22-63, 70% male). To determine the SARS-CoV-2 variants infected, saliva were collected from COVID-19 patients during onset and RNA was extracted using a QIAamp viral RNA mini kit (Qiagen, Qiagen, Cat# 52906) according to the manufacturer's protocol. The sample was subjected to whole genome sequencing based on a modified ARTIC Network protocol[60], and the near full-length SARS-CoV-2 genome sequences were obtained. Alternatively, we also performed the capture-hybridization method. The RNA isolated from saliva was treated with DNase I (Takara, Cat# EN0521) and the sequencing library was prepared using Twist library preparation kit (Twist Bioscience, Cat# 101058). The capture-hybridization was conducted using xGen COVID-19 capture panel and xGen hybridization and wash kit (Integrated DNA Technologies, Cat# 1080578) according to the manufacturer's instruction. Illumina sequencing was performed using MiSeq reagent kit v2 (300 cycles) and a MiSeq sequencer (Illumina). For the data analysis, trimmomatic-0.39[61] was used to remove the adaptors and low-quality reads from the

ACCELERATED ARTICLE PREVIEW

raw sequence data. The trimmed paired-end reads were aligned to the human genome hg38 using bowtie2 v2.3.4.3[62] and unmapped reads were mapped to the original SARS-CoV-2 genome (strain Wuhan-Hu-1, GenBank accession no. NC_045512.2) using Bwa-mem2 (https://github.com/bwa-mem2/bwa-mem2). The PCR duplicates were removed by gencore v0.16.0[63] and a consensus sequence was obtained by IGV v2.10.2[64]. The mutations detected and viral lineage were determined by using CoVsurver (https://corona.bii.a-star.edu.sg) and Pangolin COVID-19 lineage assigner (https://pangolin.cog-uk.io/). The twelve convalescent sera during early pandemic (until April 2020) (average age: 71, range: 52-92, 8% male) were purchased from RayBiotech. Sera were inactivated at 56°C for 30 min and stored at –80°C until use.

*3D Nasal epithelial cell (*hNEC*) infection*

Primary human nasal epithelial cells (Cat# EP02, Batch# MP0010) were purchased from Epithelix and maintained according to the manufacturer's procedure. The infection experiment using primary human nasal epithelial cells was performed as follows. Briefly, the working Omicron (EPI_ISL_7418017) and Delta (EPI_ISL_2378732) viruses were diluted with Opti-MEM (Thermo Fisher Scientific, Cat# 11058021). The diluted viruses (1,000 TCID50 in 100 µl) were inoculated onto the apical side of the culture and incubated at 37°C for 1 h. The inoculated viruses were removed and washed twice with Opti-MEM. To harvest the viruses on the apical side of the culture, 100 µl Opti-MEM was applied onto the apical side of the culture and incubated at 37°C for 10 min. The Opti-MEM applied was harvested and used for RT–qPCR to quantify the viral RNA copy number (see below).

Caco gut cell infection

Caco-2 Npro cells were prepared in 48-well plates and infected in biological triplicates with either SARS-CoV-2 Delta (EPI_ISL_1731019) or Omicron (M21021166) variant at m.o.i. 1 or 0.1 TCID50 per cell in 250 µl DMEM containing 2% FBS for 2 h at 37 °C with 5% CO2. Unabsorbed inoculum was then removed, cells were washed and the media was replaced with DMEM containing 2% FBS. Virus infections were maintained up to 72 h. Cell culture supernatants were harvested at 0, 24, and 48 h post infection (p.i.) where viral RNAs were extracted and quantitated by RT-qPCR using specific primer probe against E gene. An absolute quantitation against a standard curve generated was carried out using in vitro-transcribed RNA from fragment 11 clone kindly provided by Volker Thiel (University of Bern). Data were collected using a ViiA 7 Real-Time PCR System (Applied Biosystems).

ACCELERATED ARTICLE PREVIEW

Additionally, ten-fold serial dilutions of collected virus supernatants were prepared in DMEM culture media for measuring the infectious dose by 50% tissue culture infectious dose (TCID50). Virus titres were recorded at 72 hours p.i.for CPE appearance and expressed as TCID50 /ml values by the Reed–Muench method .

Calu-3 lung cell and HeLa-ACE2-TMPRSS2 live virus infection

One day before infection, Calu-3 cells (20,000 cells) and HeLa-ACE2/TMPRSS2 cells (10,000 cells) were seeded into a 96-well plate. SARS-CoV-2 [100 TCID50 for HeLa-ACE2/TMPRSS2 cells; and 2,000 TCID50 for Calu-3 cells] Omicron (EPI_ISL_7418017) or Delta (EPI_ISL_1731019) was inoculated and incubated at 37°C for 1 h. The infected cells were washed, and 180 µl of culture medium was added. The culture supernatant (10 µl) was harvested at the indicated time points and used for real-time RT-PCR to quantify viral RNA copy number [52,59]. Briefly, 5 µl of culture supernatant was mixed with 5 µl of 2 × RNA lysis buffer [2% Triton X-100, 50 mM KCl, 100 mM Tris-HCl (pH 7.4), 40% glycerol, 0.8 U/µl recombinant RNase inhibitor (Takara, Cat# 2313B)] and incubated at room temperature for 10 min. RNase-free water (90 µl) was added, and the diluted sample (2.5 µl) was used as the template for real-time RT-PCR performed according to the manufacturer's protocol using the One Step TB Green PrimeScript PLUS RT-PCR kit (Takara, Cat# RR096A) and the following primers: Forward *N*, 5'-AGC CTC TTC TCG TTC CTC ATC AC-3'; and Reverse *N*, 5'-CCG CCA TTG CCA GCC ATT C-3'. The viral RNA copy number was standardized with a SARS-CoV-2 direct detection RT-qPCR kit (Takara, Cat# RC300A). Fluorescent signals were acquired using a QuantStudio 3 Real-Time PCR system (Thermo Fisher Scientific), a CFX Connect Real-Time PCR Detection system (Bio-Rad), an Eco Real-Time PCR System (Illumina) or a 7500 Real Time PCR System (Applied Biosystems).

Western blot on infected cells and virions

VeroE6-ACE2/TMPRSS2 cells were infected with Delta (EPI_ISL_1731019), Omicron isolate 1 (M21021166) and 2 (EPI_ISL_7886688) at MOI 1. At 24 and 48 h.p.i., cells and culture media were harvested. The culture media were centrifuged with supernatants collected . To pellet down SARS-CoV-2 in the supernatants, an equal volume of clarified supernatants was mixed with 20% PEG6000 in PBS and centrifuged at 12,000 g for 30 min at 4 °C[54], followed by pellet resuspension in 1 x SDS sample buffer.

ACCELERATED ARTICLE PREVIEW

For cell lysates, the harvested cells were washed and lysed in lysis buffer (Cell Signalling) and lysates were diluted with 4 × sample buffer (Biorad) and boiled for 10 m before subjected to Western blotting. For protein detection, the following antibodies were used: rabbit anti-SARS-CoV-2 S monoclonal antibody (PA1-41165; Thermofisher), mouse anti-SARS-CoV-2 S1 (MAB105403, R&D systems), rabbit anti-SARS-CoV-2 N monoclonal antibody (clone HL344, GeneTex, GTX635679), rabbit anti-GAPDH polyclonal antibody (10494-1-AP; Proteintech), horseradish peroxidase (HRP)-conjugated anti-rabbit and anti-mouse IgG polyclonal antibody (Cell Signalling). Chemiluminescence was detected using ChemiDoc Touch Imaging System (Bio-Rad). The cleavage ratio of S1 or S2 to FL in virions was determined by densitometry using ImageJ (NIH)

Pseudotype virus preparation for testing against vaccine elicited antibodies and cell entry
Plasmids encoding the spike protein of SARS-CoV-2 D614 with a C terminal 19 amino acid deletion with D614G were used. Omicron and Delta spikes were generated by gene synthesis. Viral vectors were prepared by transfection of 293T cells by using Fugene HD transfection reagent (Promega). 293T cells were transfected with a mixture of 11ul of Fugene HD, 1μg of pCDNAΔ19 spike, 1ug of p8.91 HIV-1 gag-pol expression vector and 1.5μg of pCSFLW (expressing the firefly luciferase reporter gene with the HIV-1 packaging signal). Viral supernatant was collected at 48 and 72h after transfection, filtered through 0.45um filter and stored at -80˚C as previously described. Infectivity was measured by luciferase detection in target cells.

Neutralisation titre analyses
Neutralisation by vaccine-elicited antibodies after two doses of the BNT162b2 and Chad-Ox-1 vaccine, in addition to a third dose with BNT162b2 was determined by PV infections in the presence of serial dilutions of sera. The ID50 within groups were summarised as a geometric mean titre (GMT) and statistical comparison between groups were made with Mann-Whitney or Wilcoxon ranked sign tests. Statistical analyses were performed using Stata v13 and Prism v9.

Preparation of Monoclonal Antibodies
Casirivimab and Imdevimab were prepared as previously described[65]. To construct the plasmids expressing anti-SARS-CoV-2 monoclonal antibodies (Casirivimab and Imdevimab), the sequences of the variable regions of Casirivimab and Imdevimab were

ACCELERATED ARTICLE PREVIEW

obtained from KEGG Drug Database (https://www.genome.jp/kegg/drug/) and were artificially synthesized (Fasmac). The obtained coding sequences of the variable regions of the heavy and light chains were cloned into the pCAGGS vector containing the sequences of the human immunoglobulin 1 and kappa constant region [kindly provided by Dr. Hisashi Arase (Osaka University, Japan)].

To prepare these monoclonal antibodies, the pCAGGS vectors containing the sequences encoding the immunoglobulin heavy and light chains were cotransfected into HEK293T cells using PEI Max (Polysciences, Cat# 24765-1). At 48 h post transfection, the cell culture supernatants were harvested, and the antibodies were purified using NAb protein A plus spin kit (Thermo Fisher Scientific, Cat# 89948) according to the manufacturer's protocol.

Neutralisation Assay for monoclonal antibodies with live virus

One day prior to infection, VeroE6/TMPRSS2 (10,000 cells) were seeded into a 96-well plate. The monoclonal antibodies (Casirivimab, Imdevimab, or Casirivimab/Imdevimab) and the heat-inactivated human sera were serially diluted with DMEM supplemented with 10% FCS and 1% PS. The diluted antibodies and sera were incubated with SARS-CoV-2 (120 $TCID_{50}$) Omicron (EPI_ISL_7418017) or Delta (EPI_ISL_2378732) isolates at 37°C for 1 h. The viruses without antibodies or sera were included as controls. The mixture (containing the virus at 100 $TCID_{50}$) was inoculated onto a monolayer of VeroE6/TMPRSS2 cells and incubated at 37°C for 1 h. Then, the cells were washed with DMEM and cultured in DMEM supplemented with 10% FCS and 1% PS. At 24 h post infection, the culture supernatants were harvested and viral RNA was quantified by real-time RT-PCR. The assay of each antibody or serum was performed in triplicate or quadruplicate, and the 50% neutralization titre was calculated using Prism 9 (GraphPad Software).

Antiviral drug assay with live virus

One day prior to infection, HOS-ACE2-TMPRSS2 cells (10,000 cells) were seeded into a 96-well plate. The cells were infected with SARS-CoV-2 (100 $TCID_{50}$) Omicron (EPI_ISL_7418017) or Delta (EPI_ISL_2378732) isolates at 37°C for 1 h. Then, the cells were washed with DMEM and cultured in DMEM supplemented with 10% FCS and 1% PS and the serially diluted Remdesivir (Selleck, Cat# S8932) or beta-d-N4-hydroxycytidine (a derivative of Molnupiravir; Cell Signalling Technology, Cat# 81178S). At 24 h postinfection, the culture supernatants were harvested and viral RNA was quantified by real-time RT-PCR .

ACCELERATED ARTICLE PREVIEW

The assay of each compound was performed in quadruplicate, and the 50% neutralization titre was calculated using Prism 9 (GraphPad Software).

Cytotoxicity Assay

The CPE of the Remdesivir and beta-d-N4-hydroxycytidine were tested using a cell counting kit-8 (Dojindo, Cat# CK04-11) according to the manufacturer's instructions. One day prior to the assay, HOS-ACE2-TMPRSS2 cells (10,000 cells) were seeded into a 96-well plate. The cells were cultured with the serially diluted compound for 24 hours. The cell counting kit-8 solution (10 µl) was added to each well, and the cells were incubated at 37°C for 90 m. Absorbance was measured at 450 nm by GloMax explorer microplate reader (Promega).

PV SG-PERT and infectivity

The Delta and Omicron spike-pseudotyped viruses were prepared as described in the PV neutralisation section and standardised using a SYBR Green-based product-enhanced PCR assay (SG-PERT) as described previously. [66]. Briefly, 10-fold dilutions of virus supernatant were lysed in a 1:1 ratio in a 2x lysis solution (made up of 40% glycerol v/v 0.25% Triton X-100 v/v 100mM KCl, RNase inhibitor 0.8 U/ml, TrisHCL 100mM, buffered to pH7.4) for 10 minutes at room temperature. Sample lysates (12 µl) were added to 13 µl of SYBR Green master mix (containing 0.5µM of MS2-RNA Fwd and Rev primers, 3.5pmol/ml of MS2-RNA, and 0.125U/µl of Ribolock RNAse inhibitor and cycled in a QuantStudio. Relative amounts of reverse transcriptase activity were determined as the rate of transcription of bacteriophage MS2 RNA, with absolute RT activity calculated by comparing the relative amounts of RT to an RT standard of known activity.

PV were used to transduce different target cell lines and 3D organoid cultures. After 48 or 72 hr post transduction, the cells were lysed with direct addition of Bright Glo (Promega). The raw readings were then normalised against the SG-PERT and plotted using GraphPad Prism.

Entry Inhibitors in A549-ACE2-TMPRSS2 cells with PV and live virus

A549-ACE2-TMPRSS2 (A549-A2T2) cells were either E64D (Tocris) or camostat (Sigma-Aldrich) treated for 2 hours at each drug concentration before the addition of a comparable amount of input viruses pseudotyped with Delta or Omicron (approx. 100,000 RLU). The cells were then left for 48 hours before addition of substrate for luciferase (Promega) and read on a Glomax plate reader (Promega).

ACCELERATED ARTICLE PREVIEW

Quantification of viral replication in A549-ACE2-TMPRSS2-based luminescent reporter cells was performed as previously described[67] and Gerber et al., *manuscript in preparation*). In brief, A549-A2T2 reporter cells (clone E8) over-expressing Renilla luciferase (Rluc) and SARS-CoV-2 Papain-like protease-activatable circularly permuted firefly luciferase (FFluc) were seeded in flat-bottomed 96-well plates. The following morning, cells were treated with the indicated doses of Camostat or E64d for 2 h, then infected with Delta (EPI_ISL_1731019) or Omicron (M21021166) variants of SARS-CoV-2 at MOI = 0.01. After 24 h, cells were lysed in Dual-Glo Luciferase Buffer (Promega) diluted 1:1 with PBS and 1% NP-40. Lysates were then transferred to opaque 96-well plates, and viral replication quantitated as the ratio of FFluc/Rluc luminescence measured using the Dual-Glo kit (Promega) according to the manufacturer's instructions. % inhibition was calculated relative to the maximum luminescent signal for each condition, then analysed using the Sigmoidal, 4PL, X is log(concentration) function in GraphPad Prism.

Immunofluorescence (IF) assays

HeLa-ACE2 cells were grown on 19 mm glass coverslips in 24-well plates and infected with Delta and Omicron for 24 h. Cells were fixed in 4% paraformaldehyde (Applichem GmbH, Germany), and permeabilised in PBS-T (0.1% v/v Triton X-100 in PBS) for 5 min. Cells were blocked in PBS-T containing 5% w/v BSA for 30 min and labelled with primary antibodies against SARS-CoV-2 Spike (GTX632604**,**) or anti-GM130[EP892Y]-cis-Golgi (ab52649) in PBS-T, 1% w/v BSA for 1 h at room temperature. After washing, cells were stained with fluorochrome-conjugated secondary antibodies in PBS-T, 1% w/v BSA for 1 h at room temperature in the dark. Nuclei were counterstained with 4',6'-diamidino-2-phenylindole dihydrochloride (DAPI) and phalloidin 647 (A22287, Molecular Probes, Germany). Confocal images were acquired on a Leica TCS SP8 microscope. Post-acquisition analysis was performed using Leica LAS X or Fiji (v1.49) software. For distance analysis, the two-dimensional coordinates of the centroids of Spike proteins were calculated using the Analyze Particles module of Fiji (ImageJ). The distance of each particle to the edge of the nucleus, visualised using DAPI stain, was looked up using a Euclidean distance map computed with the Distance Transform module of Fiji and exported as a list of distance measurements via the Analyze Particle function. Colocalization of Spike with the Golgi were estimated through Pearson's correlation coefficients (*R*) using the PSC colocalization plug-in (ImageJ, NIH). *R* values between −1 (perfect negative correlation) and +1 (perfect positive

ACCELERATED ARTICLE PREVIEW

correlation), with 0 corresponding to no correlation were assigned[68]. Colocalization analyses were performed on >20 cells.

Cell-cell fusion assay

Cell-cell fusion assays were carried out as follows. Briefly, 293T GFP11and Vero-GFP1-10 cells were seeded at 80% confluence in a 1:1 ration in 48 multiwell plate the day before. Cells were co-transfected with 0.5 µg of spike expression plasmids in pCDNA3 using Fugene 6 following the manufacturer's instructions (Promega). Cell-cell fusion was measured using an Incucyte and determined as the proportion of green area to total phase area. Graphs were generated using Prism 8 software. To measure cell surface spike expression HEK293 cells were transfected with S expression plasmids and stained with rabbit anti-SARS-CoV-2 S S1/S2 polyclonal antibody (Thermo Fisher Scientific, Cat# PA5-112048, 1:100). Normal rabbit IgG (SouthernBiotech, Cat# 0111-01, 1:100) was used as a negative control, and APC-conjugated goat anti-rabbit IgG polyclonal antibody (Jackson ImmunoResearch, Cat# 111-136-144, 1:50) was used as a secondary antibody. Surface expression level of S proteins was analysed using FACS Canto II (BD Biosciences) and FlowJo software v10.7.1 (BD Biosciences). Gating strategy for flow cytometry is shown in Supplementary Figure 8.

Analysis of size of infection foci

Vero E6 cells (ATCC CRL-1586, obtained from Cellonex in South Africa) were propagated in complete growth medium consisting of Dulbecco's Modified Eagle Medium (DMEM) with 10% fetal bovine serum (Hyclone) containing 10mM of HEPES, 1mM sodium pyruvate, 2mM L-glutamine and 0.1mM nonessential amino acids (Sigma-Aldrich). Vero E6 cells were passaged every 3–4 days. H1299 cell lines were propagated in growth medium consisting of complete Roswell Park Memorial Institute (RPMI) 1640 medium with 10% fetal bovine serum containing 10mM of HEPES, 1mM sodium pyruvate, 2mM L-glutamine and 0.1mM nonessential amino acids. H1299 cells were passaged every second day. The H1299-E3 (H1299-ACE2, clone E3) cell line was derived from H1299 (CRL-5803).

Virus stock using a South Africa (EPI_ISL_7886688) derived isolate, and Delta variant isolate, was produced as described[2] and used at approximately 50-100 focus-forming units per microwell. H1299-E3 cells were plated in a 96-well plate (Corning) at 30,000 cells per well 1 day pre-infection. Cells were infected with 100 µL of the virus working stock for 1 h, then 100 µL of a 1X RPMI 1640 (Sigma-Aldrich, R6504), 1.5% carboxymethylcellulose

ACCELERATED ARTICLE PREVIEW

(Sigma-Aldrich, C4888) overlay was added without removing the inoculum. Cells were fixed 2 h or 18 h post-infection using 4% PFA (Sigma-Aldrich) for 20 min. Foci were stained with a rabbit anti-spike monoclonal antibody (BS-R2B12, GenScript A02058) at 0.5 μg/mL in a permeabilization buffer containing 0.1% saponin (Sigma-Aldrich), 0.1% BSA (Sigma-Aldrich) and 0.05% Tween-20 (Sigma-Aldrich) in PBS. Plates were incubated with primary antibody overnight at 4 °C, then washed with wash buffer containing 0.05% Tween-20 in PBS. Secondary goat anti-rabbit HRP conjugated antibody (Abcam ab205718) was added at 1 μg/mL and incubated for 2 h at room temperature with shaking. TrueBlue peroxidase substrate (SeraCare 5510-0030) was then added at 50 μL per well and incubated for 20 min at room temperature. Plates were imaged in an ImmunoSpot Ultra-V S6-02-6140 Analyzer ELISPOT instrument with BioSpot Professional built-in image analysis (C.T.L). For microscopy, wells were imaged using a Metamorph-controlled Nikon TiE motorized microscope with a 10x objective. Automated image analysis was performed using a custom script in Matlab 2019b. Statistics and graphing performed by Prism version 8.0.

Reporting summary

Further information on research design is available in the Nature Research Reporting Summary linked to this paper.

Data availability:

The sequences of the virus isolates used are available in GISAID: **B.1.1.617.2** (Delta, GISAID accession no. EPI_ISL_1731019), **B.1.1.529** (Omicron BA.1 isolate from UK, M21021166), **B.1.1.529** (Omicron BA.1 isolate from South Africa, GISAID accession no EPI_ISL_7886688), and (BA.1 isolate from Japan, GISAID ID: EPI_ISL_7418017).
The structural models used in this study for Delta and Omicron variants are available at https://github.com/CSB-Thukral-Lab/Spike_structural_models_Delta_and_Omicron, and at https://github.com/ojcharles/viral_alphafold. The data for single-cell RNA-sequencing data analysis is available in github: https://github.com/elo073/Lung5loc_scRNAseq_omcr_entrygenes.

Code availability

The code for single-cell RNA-sequencing data analysis is available in github: https://github.com/elo073/Lung5loc_scRNAseq_omcr_entrygenes

ACCELERATED ARTICLE PREVIEW

43 Katoh, K. & Standley, D. M. MAFFT multiple sequence alignment software version 7: improvements in performance and usability. *Mol Biol Evol* **30**, 772-780, doi:10.1093/molbev/mst010 (2013).
44 Jumper, J. *et al.* Highly accurate protein structure prediction with AlphaFold. *Nature* **596**, 583-589, doi:10.1038/s41586-021-03819-2 (2021).
45 Goddard, T. D. *et al.* UCSF ChimeraX: Meeting modern challenges in visualization and analysis. *Protein Science* **27**, 14-25 (2018).
46 Walls, A. C. *et al.* Structure, Function, and Antigenicity of the SARS-CoV-2 Spike Glycoprotein. *Cell* **181**, 281-292 e286, doi:10.1016/j.cell.2020.02.058 (2020).
47 McCallum, M. *et al.* Molecular basis of immune evasion by the Delta and Kappa SARS-CoV-2 variants. *Science* **374**, 1621-1626, doi:10.1126/science.abl8506 (2021).
48 Starr, T. N. *et al.* Deep Mutational Scanning of SARS-CoV-2 Receptor Binding Domain Reveals Constraints on Folding and ACE2 Binding. *Cell* **182**, 1295-1310 e1220, doi:10.1016/j.cell.2020.08.012 (2020).
49 Cathcart, A. L. *et al.* The dual function monoclonal antibodies VIR-7831 and VIR-7832 demonstrate potent in vitro and in vivo activity against SARS-CoV-2. *bioRxiv*, 2021.2003.2009.434607, doi:10.1101/2021.03.09.434607 (2021).
50 Madissoon, E. *et al.* A spatial multi-omics atlas of the human lung reveals a novel immune cell survival niche. *bioRxiv*, 2021.2011.2026.470108, doi:10.1101/2021.11.26.470108 (2021).
51 Motozono, C. *et al.* SARS-CoV-2 spike L452R variant evades cellular immunity and increases infectivity. *Cell host & microbe* **29**, 1124-1136 e1111, doi:10.1016/j.chom.2021.06.006 (2021).
52 Saito, A. *et al.* Enhanced fusogenicity and pathogenicity of SARS-CoV-2 Delta P681R mutation. *Nature*, doi:10.1038/s41586-021-04266-9 (2021).
53 Matsuyama, S. *et al.* Enhanced isolation of SARS-CoV-2 by TMPRSS2-expressing cells. *Proceedings of the National Academy of Sciences of the United States of America* **117**, 7001-7003, doi:10.1073/pnas.2002589117 (2020).
54 Papa, G. *et al.* Furin cleavage of SARS-CoV-2 Spike promotes but is not essential for infection and cell-cell fusion. *PLoS pathogens* **17**, e1009246, doi:10.1371/journal.ppat.1009246 (2021).
55 Brevini, T. *et al.* FXR inhibition reduces ACE2 expression, SARS-CoV-2 infection and may improve COVID-19 outcome. *bioRxiv*, 2021.2006.2006.446781, doi:10.1101/2021.06.06.446781 (2021).
56 Youk, J. *et al.* Three-Dimensional Human Alveolar Stem Cell Culture Models Reveal Infection Response to SARS-CoV-2. *Cell Stem Cell* **27**, 905-919 e910, doi:10.1016/j.stem.2020.10.004 (2020).
57 Dejnirattisai, W. *et al.* Omicron-B.1.1.529 leads to widespread escape from neutralizing antibody responses. *bioRxiv*, doi:10.1101/2021.12.03.471045 (2021).
58 Dejnirattisai, W. *et al.* Reduced neutralisation of SARS-CoV-2 omicron B.1.1.529 variant by post-immunisation serum. *Lancet* **399**, 234-236, doi:10.1016/S0140-6736(21)02844-0 (2022).
59 Motozono, C. *et al.* SARS-CoV-2 spike L452R variant evades cellular immunity and increases infectivity. *Cell Host Microbe* **29**, 1124-1136, doi:10.1016/j.chom.2021.06.006 (2021).

ACCELERATED ARTICLE PREVIEW

60 Itokawa, K., Sekizuka, T., Hashino, M., Tanaka, R. & Kuroda, M. Disentangling primer interactions improves SARS-CoV-2 genome sequencing by multiplex tiling PCR. *PLoS One* **15**, e0239403, doi:10.1371/journal.pone.0239403 (2020).
61 Bolger, A. M., Lohse, M. & Usadel, B. Trimmomatic: a flexible trimmer for Illumina sequence data. *Bioinformatics* **30**, 2114-2120, doi:10.1093/bioinformatics/btu170 (2014).
62 Langmead, B. & Salzberg, S. L. Fast gapped-read alignment with Bowtie 2. *Nat Methods* **9**, 357-359, doi:10.1038/nmeth.1923 (2012).
63 Chen, S. *et al.* Gencore: an efficient tool to generate consensus reads for error suppressing and duplicate removing of NGS data. *BMC Bioinformatics* **20**, 606, doi:10.1186/s12859-019-3280-9 (2019).
64 Thorvaldsdottir, H., Robinson, J. T. & Mesirov, J. P. Integrative Genomics Viewer (IGV): high-performance genomics data visualization and exploration. *Brief Bioinform* **14**, 178-192, doi:10.1093/bib/bbs017 (2013).
65 Kimura, I. *et al.* SARS-CoV-2 Lambda variant exhibits higher infectivity and immune resistance. *BioRxiv*, 454085 (2021).
66 Vermeire, J. *et al.* Quantification of reverse transcriptase activity by real-time PCR as a fast and accurate method for titration of HIV, lenti- and retroviral vectors. *PloS one* **7**, e50859-e50859, doi:10.1371/journal.pone.0050859 (2012).
67 Gerber, P. P. *et al.* A protease-activatable luminescent biosensor and reporter cell line for authentic SARS-CoV-2 infection. *bioRxiv*, 2021.2003.2022.435957, doi:10.1101/2021.03.22.435957 (2021).
68 French, A. P., Mills, S., Swarup, R., Bennett, M. J. & Pridmore, T. P. Colocalization of fluorescent markers in confocal microscope images of plant cells. *Nat Protoc* **3**, 619-628, doi:10.1038/nprot.2008.31 (2008).

Acknowledgements RKG is supported by a Wellcome Trust Senior Fellowship in Clinical Science (WT108082AIA). IG is a Wellcome Senior Fellow (207498/Z/17/Z). This study was supported by the Cambridge NIHRB Biomedical Research Centre. I.A.T.M.F. is funded by a SANTHE award (DEL-15-006). AA is supported by a Africa Research Excellence Fund Research Development Fellowship (AREF-318-ABDUL-F-C0882). We would like to thank Paul Lehner for Calu-3 cells. We would like to thank James Voss for HeLa ACE2 and Suzanne Rihn for the A549 cells. We thank Gavin Screaton for the Omicron isolate M21021166. We would like to thank Claire Cormie for microscope training, Anna Albecka for advice on SARS-CoV2 virion purification, and Khadija Khan for work on foci. We would like to thank Thushan de Silva for the Delta variant isolate. This work was supported by the MRC (TSF ref. MR/T032413/1 to NJM), NHSBT (grant ref. WPA15-02 to NJM), Addenbrooke's Charitable Trust (grant ref. to 900239 NJM). The authors acknowledge support from the G2P-UK National Virology consortium funded by MRC/UKRI (grant ref:

ACCELERATED ARTICLE PREVIEW

MR/W005611/1), and thank Tom Peaccok and Wendy Barclay. This study was also supported by The Rosetrees Trust and the Geno2pheno UK consortium. SF acknowledges the EPSRC (EP/V002910/1). KS is supported by AMED Research Program on Emerging and Re-emerging Infectious Diseases (20fk0108270 and 20fk0108413), JST SICORP (JPMJSC20U1 and JPMJSC21U5) and JST CREST (JPMJCR20H4). We would like to thank all members belonging to The Genotype to Phenotype Japan (G2P-Japan) Consortium. We thank National Institute for Infectious Diseases, Japan and Hisashi Arase (Osaka University, Japan) for providing virus isolates and reagents and Ituro Inoue and Sachiko Sakamoto (National Institute of Genetics, Japan) for technical supports. This study was supported in part by AMED Research Program on Emerging and Re-emerging Infectious Diseases 20fk0108163 (to Akatsuki Saito), 20fk0108146 (to Kei Sato), 20fk0108270 (to Kei Sato), 20fk0108413 (to Terumasa Ikeda and Kei Sato) and 20fk0108451 (to Akatsuki Saito, Terumasa Ikeda, Takamasa Ueno, Akifumi Takaori-Kondo, G2P-Japan Consortium and Kei Sato); AMED Research Program on HIV/AIDS 21fk0410033 (to Akatsuki Saito) and 21fk0410039 (to Kei Sato); AMED Japan Program for Infectious Diseases Research and Infrastructure 20wm0325009 (to Akatsuki Saito) and 21wm0325009 (to Akatsuki Saito); JST A-STEP JPMJTM20SL (to Terumasa Ikeda); JST SICORP (e-ASIA) JPMJSC20U1 (to Kei Sato); JST SICORP JPMJSC21U5 (to Kei Sato), JST CREST JPMJCR20H4 (to Kei Sato); JSPS KAKENHI Grant-in-Aid for Scientific Research C 19K06382 (to Akatsuki Saito), Scientific Research B 18H02662 (to Kei Sato) and 21H02737 (to Kei Sato); JSPS Fund for the Promotion of Joint International Research (Fostering Joint International Research) 18KK0447 (to Kei Sato); JSPS Core-to-Core Program JPJSCCA20190008 (A. Advanced Research Networks) (to Kei Sato); JSPS Research Fellow DC1 19J20488 (to Izumi Kimura); JSPS Leading Initiative for Excellent Young Researchers (LEADER) (to Terumasa Ikeda); Takeda Science Foundation (to Terumasa Ikeda); The Tokyo Biochemical Research Foundation (to Kei Sato); Mitsubishi Foundation (to Terumasa Ikeda); Shin-Nihon Foundation of Advanced Medical Research (to Terumasa Ikeda); a Grant for Joint Research Projects of the Research Institute for Microbial Diseases, Osaka University (to Akatsuki Saito) ; an intramural grant from Kumamoto University COVID-19 Research Projects (AMABIE) (to Terumasa Ikeda); Intercontinental Research and Educational Platform Aiming for Eradication of HIV/AIDS (to Terumasa Ikeda); and Joint Usage/Research Center program of Institute for Frontier Life and Medical Sciences, Kyoto University (to Kei Sato). This study was supported by the National Institute of Allergy and Infectious Diseases

ACCELERATED ARTICLE PREVIEW

(DP1AI158186 and HHSN272201700059C to D.V.), a Pew Biomedical Scholars Award (D.V.), an Investigators in the Pathogenesis of Infectious Disease Awards from the Burroughs Wellcome Fund (D.V.), Fast Grants (D.V.) and the Bill and Melinda Gates Foundation (OPP1156262 to D.V.). D.V. is an Investigator of the Howard Hughes Medical Institute. T.B. is supported by an EASL Juan Rodès fellowship. F.S. was supported by a UKRI Future Leaders fellowship. AS was supported by the Bill and Melinda Gates award INV-018944, National Institutes of Health award R01 AI138546 and South African Medical Research Council award. The National Institute of General Medical Sciences (5T32GM008268-32 to SKZ). Studies using human donor lung tissue were supported by the NIHR Blood and Transplant Research Unit (BTRU) in Organ Donation and Transplantation at Newcastle University and the University of Cambridge and in partnership with NHS Blood and Transplant (NHSBT). The views expressed are those of the author(s) and not necessarily those of the NIHR, the Department of Health and Social Care or NHSBT.

Author contributions Conceived research and designed study: R.K.G., K.S., B.M. N.J.M., I.G.G., designed experiments: D.C, M.S.P., A.D.M., B.M., R.K.G., N.G., M.H. I.G.G, J.H.L., A.T-K., K.S., T.U., S.M., J.K., T.S.T, M.T., S.K.Z., A.C.W., D.V, F.S., A.S., L.C.J, A.J.F., S.A.T., R.D., J.B., J.A.G.B., K.G.C.S; Performed experiments: B.M., A.A., I.A.T.M., N.G., S.K.Z, A.D.M., S.A.K., S.F., S.R., P.P.G., D.Y., I.K., A.S., G.P., O.J.C., D.L.M., T.B., A.T-K., I.K., K.S., T.U., S.M., J.K., T.S.T, M.T., T.I., J.E.B, A.J., L.C-G, P.M., E.M., Analysed data: SKZ, N.G., ACW, DV, R.K.G, B.M, I.G.G., N.J.M, P.P.G., D.Y., I.K., A.S., D.V., A.T-K., K.S., T.U., S.M., J.K., T.S.T, M.T., A.S., K.M., M.S.P.; R.K.G., D.V. and B.M wrote the manuscript with input from all authors.

Competing interests M.S.P., D.C. and A.d.M are employees of Vir Biotechnology and may hold shares in Vir Biotechnology. RKG has received honoraria for educational activities from Johnson & Johnson, ViiV and GSK. F.S. is shareholder in Bilitech LTD. The Veesler lab has received an unrelated research sponsored agreement from Vir Biotechnology Inc.Remaining authors have no competing interests to declare.

Additional information
Supplementary information is available for this paper at
Correspondence and requests for materials should be addressed to Kei Sato and Ravindra K. Gupta.
Peer review information *Nature* thanks the anonymous reviewers for their contribution to the peer review of this work. Peer reviewer reports are available.
Reprints and permissions information is available at www.nature.com/reprints.

ACCELERATED ARTICLE PREVIEW

Ecuador-COVID19 Consortium

Paúl Cárdenas[29], Erika Muñoz[29], Veronica Barragan[29], Sully Márquez[29], Belén Prado-Vivar[29], Mónica Becerra-Wong[29], Mateo Caravajal[29], Gabriel Trueba[29], Patricio Rojas-Silva[29], Michelle Grunauer[30], Bernardo Gutierrez[31], Juan José Guadalupe[31], Juan Carlos Fernández-Cadena[32], Derly Andrade-Molina[33], Manuel Baldeon[34], Andrea Pinos[35]

[29]Universidad San Francisco de Quito, COCIBA, Instituto de Microbiología, Cumbaya EC1702, Ecuador.

[30]Universidad San Francisco de Quito, COCSA, Escuela de Medicina, Cumbaya EC1702, Ecuador.

[31]Universidad San Francisco de Quito, COCIBA, Laboratorio de Biotecnología Vegetal, Cumbaya EC1702, Ecuador.

[32]Laboratorio INTERLAB, Guayaquil EC09, Ecuador.

[33]Universidad Espíritu Santo, Laboratorio de Omicas, Guayaquil, EC09, Ecuador.

[34]Universidad Internacional del Ecuador, Facultad de Ciencias Médicas, de la Salud y la Vida, Quito EC1701, Ecuador.

[35]Centros Médicos Dr. Marco Albuja, Quito EC1701, Ecuador.

The Genotype to Phenotype Japan (G2P-Japan) Consortium members

Erika P Butlertanaka[3], Yuri L Tanaka[3], Terumasa Ikeda[5], Jumpei Ito[4], Izumi Kimura[4], Keiya Uriu[4], Yusuke Kosugi[4], Mai Suganami[4], Akiko Oide[4], Miyabishara Yokoyama[4], Mika Chiba[4], Chihiro Motozono[5], Hesham Nasser[5], Ryo Shimizu[5], Yue Yuan[5], Kazuko Kitazato[5], Haruyo Hasebe[5], So Nakagawa[36], Jiaqi Wu[36], Miyoko Takahashi[36], Takasuke Fukuhara[37], Kenta Shimizu[37], Kana Tsushima[37], Haruko Kubo[37], Yasuhiro Kazuma[38], Ryosuke Nomura[38], Yoshihito Horisawa[38], Kayoko Nagata[38], Yugo Kawai[38], Yohei Yanagida[38], Yusuke Tashiro[38], Kenzo Tokunaga[39], Seiya Ozono[39], Ryoko Kawabata[40], Nanami Morizako[40], Kenji Sadamasu[41], Hiroyuki Asakura[41], Mami Nagashima[41], Kazuhisa Yoshimura[41]

[36]Tokai University, Tokyo, Japan.

[37]Hokkaido University, Sapporo, Japan.

[38]Kyoto University, Kyoto, Japan.

[39]National Institute of Infectious Diseases, Tokyo, Japan.

ACCELERATED ARTICLE PREVIEW

[40]Institute of Biomedical and Health Sciences, Hiroshima University, Hiroshima 7348551, Japan.
[41]Tokyo Metropolitan Institute of Public Health, Tokyo 1690073, Japan.

The CITIID-NIHR BioResource COVID-19 Collaboration

Stephen Baker[1,2], Gordon Dougan[1,2], Christoph Hess[2], Nathalie Kingston[9], Paul J. Lehner[1,2], Paul A. Lyons[1,2], Nicholas J. Matheson[1,2], Willem H. Owehand[2], Caroline Saunders[42], Charlotte Summers[2,19], James E.D. Thaventhiran[19], Mark Toshner[2], Michael P. Weekes[2], Patrick Maxwell[19], Ashley Shaw[19], Ashlea Bucke[42], Jo Calder[42], Laura Canna[42], Jason Domingo[42], Anne Elmer[42], Stewart Fuller[42], Julie Harris[42], Sarah Hewitt[42], Jane Kennet[42], Sherly Jose[42], Jenny Kourampa[42], Anne Meadows[42], Criona O'Brien[42], Jane Price[42], Cherry Publico[42], Rebecca Rastall[42], Carla Ribeiro[42], Jane Rowlands[42], Valentina Ruffolo[42], Hugo Tordesillas[42], Ben Bullman[2], Benjamin J. Dunmore[2], Stuart Fawke[39], Stefan Gräf[2], Josh Hodgson[3], Christopher Huang[3], Kelvin Hunter[2,], Emma Jones[31], Ekaterina Legchenko[2], Cecilia Matara[2], Jennifer Martin[2], Federica Mescia[2], Ciara O'Donnell[2], Linda Pointon[2], Joy Shih[2], Rachel Sutcliffe[2], Tobias Tilly[2], Carmen Treacy[2], Zhen Tong[2], Jennifer Wood[2], Marta Wylot[2], Ariana Betancourt[2], Georgie Bower[2], Chiara Cossetti[2,], Aloka De Sa[2], Madeline Epping[2], Stuart Fawke[2], Nick Gleadall[2], Richard Grenfell[2], Andrew Hinch[2], Sarah Jackson[2], Isobel Jarvis[19], Ben Krishna[2], Francesca Nice[42], Ommar Omarjee[2], Marianne Perera[2], Martin Potts[2], Nathan Richoz[2], Veronika Romashova[2], Luca Stefanucci[2], Mateusz Strezlecki[2], Lori Turner[2], Eckart M.D.D. De Bie[2], Katherine Bunclark[2], Masa Josipovic[2], Michael Mackay[2], John Allison[43], Helen Butcher[42], Daniela Caputo[42,43], Debbie Clapham-Riley[42], Eleanor Dewhurst[42], Anita Furlong[42], Barbara Graves[42, 43], Jennifer Gray[40, 43], Tasmin Ivers[42], Emma Le Gresley[42,43], Rachel Linger[42], Sarah Meloy[42], Francesca Muldoon[42], Nigel Ovington[43], Sofia Papadia[42], Isabel Phelan[42], Hannah Stark[9,40], Kathleen E Stirrups[22,12], Paul Townsend[40], Neil Walker[40], Jennifer Webster[9,40], Ingrid Scholtes[40], Sabine Hein[40], Rebecca King[40]

[42]Cambridge Clinical Research Centre, NIHR Clinical Research Facility, Cambridge University Hospitals NHS Foundation Trust, Addenbrooke's Hospital, Cambridge CB2 0QQ, UK.
[43]NIHR. Bioresource, Cambridge, UK.

ACCELERATED ARTICLE PREVIEW

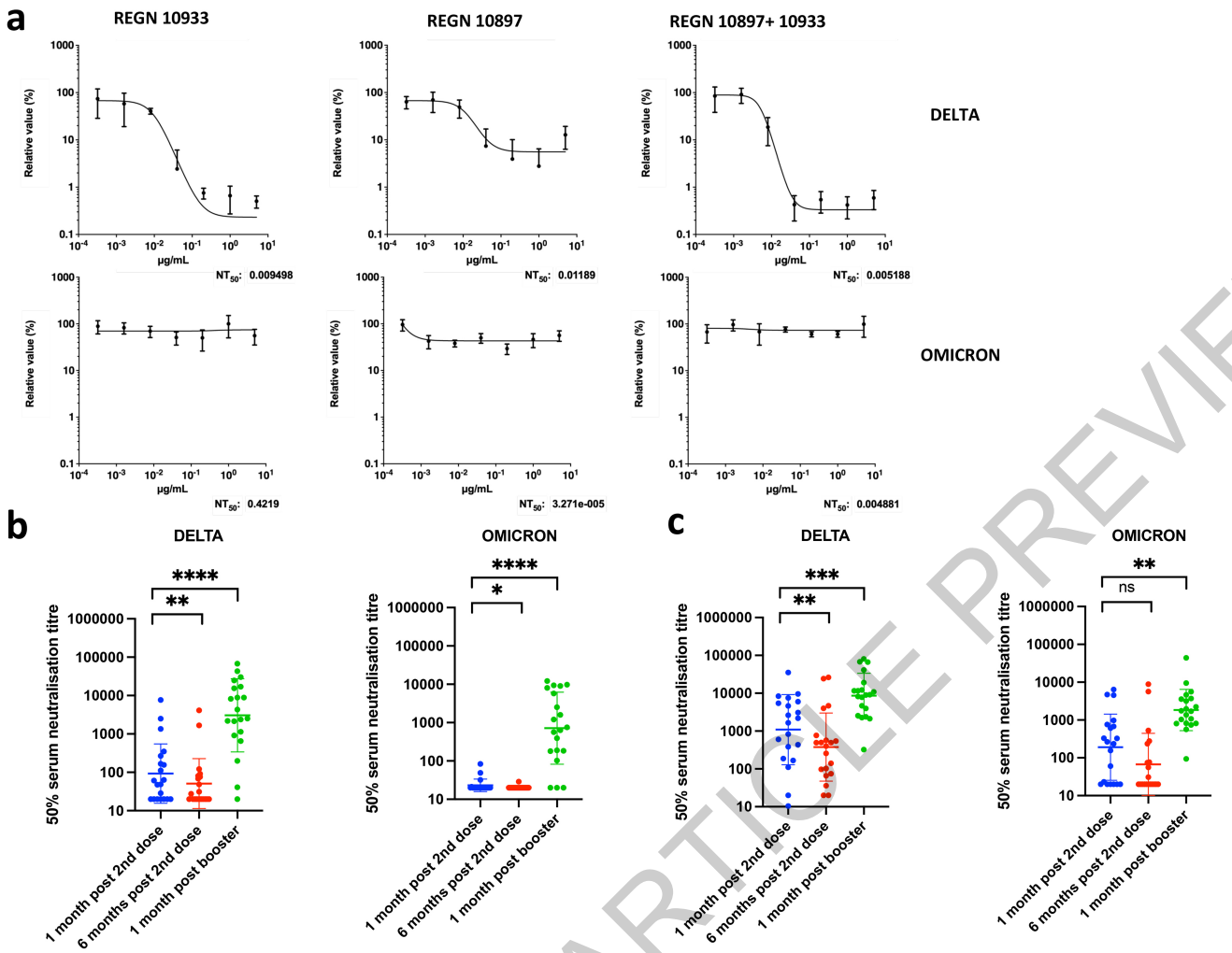

Fig. 1 Sensitivity of SARS-CoV-2 Omicron to clinically approved monoclonal antibodies and to vaccine elicited neutralizing antibodies. a. titration of monoclonal antibodies REGN 10933 and 10897 and combination of both against replication competent Delta and Omicron viruses. Data points are mean of technical replicates (n=4 at each dilution for each virus) with +/- SEM shown. Curve fitting for dose response was done in GraphPad prism. NT: Neutralising titre. **b-c**.Neutralisation of spike pseudotyped virus by sera from vaccinated individuals (**b.** n=20 ChAdOx-1 or **c.** n=20 BNT12b2) over three time points following dose two (ChAdOx-1 or BNT162b2) and dose three (BNT162b2 only). GMT (geometric mean titre) with s.d are presented. Data representative of two independent experiments each with two technical replicates. **p<0.01, *** p<0.001, ****p<0.0001 Wilcoxon matched-pairs signed rank test, ns not significant.

ACCELERATED ARTICLE PREVIEW

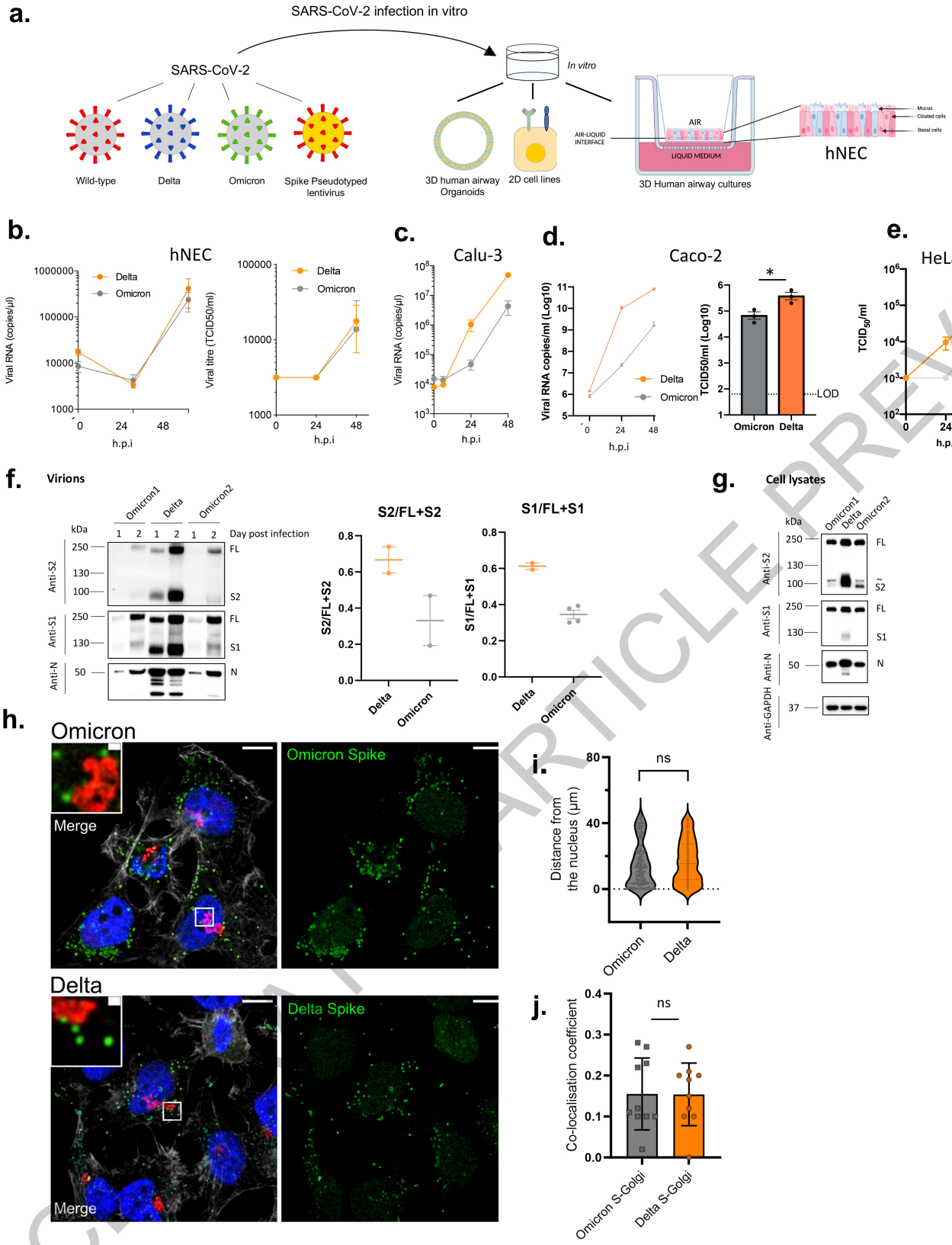

Fig. 2 | See next page for caption.

ACCEPTED ARTICLE PREVIEW

Fig. 2 SARS-CoV-2 Omicron and Delta Variant live virus replication in 3D tissue culture systems and 2D cell lines. a. overview of viruses and culture systems used; hNEC (human nasal epithelial cultures). Schematic created with BioRender.com**. b-d.** Spreading infection by replication competent Omicron versus Delta variant over time in **b**. hNEC **c.** Calu-3 **d**. Caco-2 Npro **e.** HeLa-A2T2**.** Viral RNA and/or infectious virus in supernatant (TCID50) were measured. Data are are representative of two independent experiments and mean +/- sd for technical replicates are shown. * $p<0.05$ by two-sided unpaired student t-test. **f-g.** Western blot of **f**. Two live Omicron and one Delta virus isolates probed with antibodies to S2, S1 and N with quantification of S2 and S1 to total spike ratio. Mean ratio +/- SEM is shown for 2-4 biological replicates **g.** Vero E6 A2T2 producer cell lysates infected with live isolates probed with antibodies to S2, S1 and N. Housekeeping gene GAPDH as loading control. '~' above the S2 band is a non-specific band. Data are representative of two independent experiments. **h-j**. Subcellular localisation of Spike in SARS-Cov-2 Delta vs Omicron infected cells. Subcellular distribution of Omicron, Delta Spike proteins in Hela-ACE2 cells infected with live virus isolates. **h.** Cells on coverslips were infected for 24 h, fixed and stained with anti-Spike, anti-GM130-cis-Golgi, phalloidin 647 and DAPI, and imaged on a Leica TCS SP8 confocal microscope. **i**. The distance of spike proteins from nucleus at 24 hpi. Data points (n=144 for each virus) are shown along with median and IQR. **j**. Quantitation of Spike-Golgi colocalisation in infected cells with mean +/- sd (n=10 for each virus). Values were calculated using Pearson's correlation coefficient. Scale bars: 10 μm and 1 μm, respectively. * $p<0.05$ by two-sided unpaired student t-test; NS – not significant.

ACCELERATED ARTICLE PREVIEW

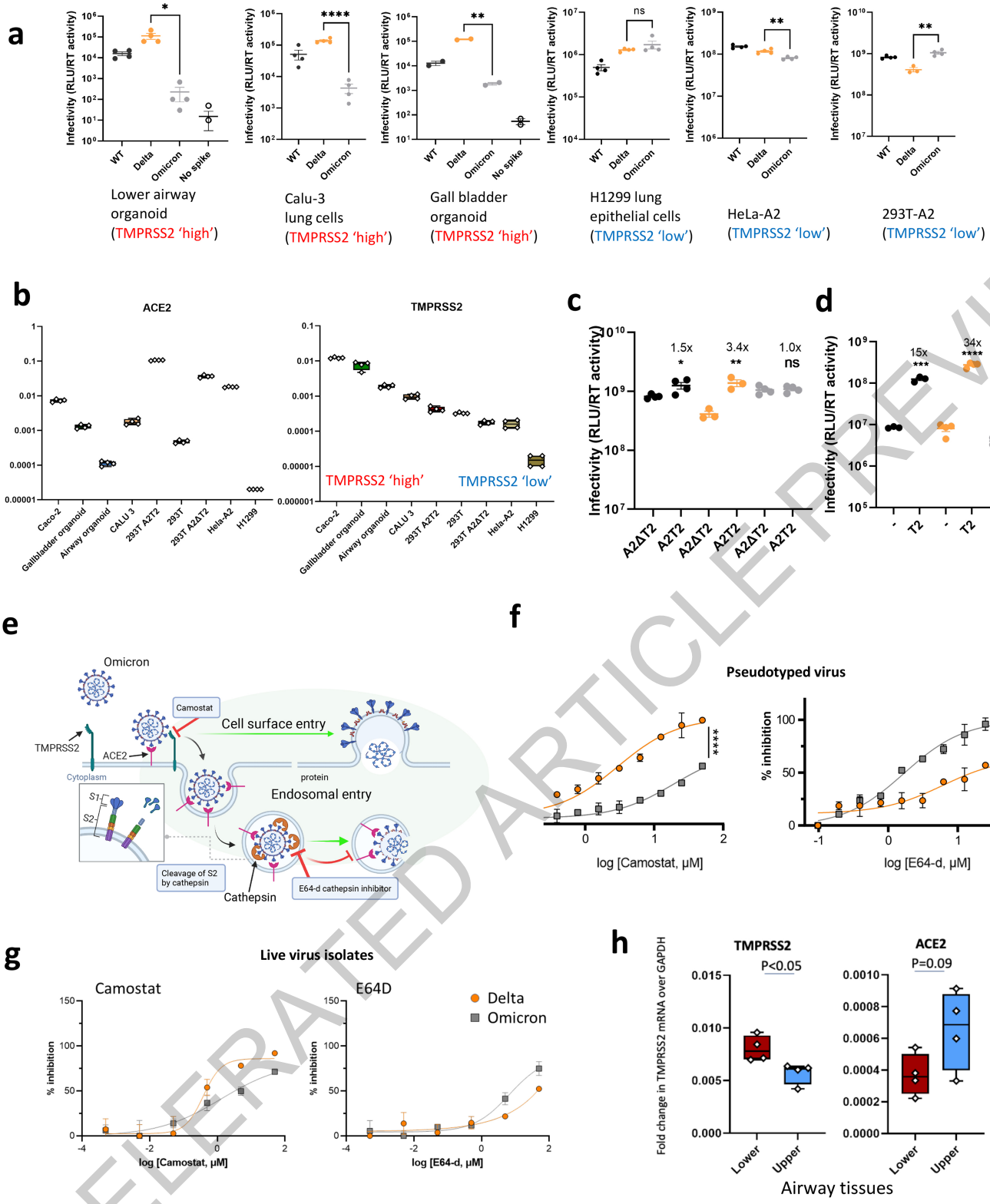

Fig. 3 | See next page for caption.

ACCELERATED ARTICLE PREVIEW

Fig. 3 SARS-CoV-2 Omicron Variant spike enters cells less efficiently by TMPRSS2 dependent plasma membrane fusion. a. PV entry in airway organoids, Calu-3 lung cells, gall bladded organoids, H1299 lung cells, HeLa-ACE2 overexpressing cells and HEK 293-ACE2 overexpressing cells. Black – WT Wuhan-1 D614G, orange – Delta B.1.617.2, grey - Omicron BA.1. mean +/- SEM are shown for technical replicates (n=2-4). Two-sided unpaired Student t test, *p<0.05, **p<0.01, ****p<0.0001. Data are representative of three independent experiments. **b.** mRNA transcripts for ACE2 and TMPRSS2 in indicated cell types and organoids as measured by qPCR. Samples were run as technical replicates (n=4), centre line median; box interquartile range (IQR), whiskers range. Data are representative of two independent experiments **c.** Entry of PV expressing spike in 293T cells transduced to overexpress ACE2 and (i) depleted for TMPRSS2 (A2Δ T2) or (ii) overexpressing TMPRSS2 (A2T2). **d.** Entry of PV expressing spike in 293T cells with endogenous (-) or overexpressed TMPRSS2 (T2). Data for **c-d** are representative of three independent experiments, with mean of technical replicates (n=4) shown +/- SEM, two-sided unpaired students t test *p<0.05, **p<0.01, ***p<0.001, ****p<0.0001. **e**. An illustration of two cell entry pathways known to be used by SARS-CoV-2. Schematic created with BioRender.com. **f.** Titration of inhibitors in A549-ACE2-TMPRSS2 cells using PV expressing Delta (orange) or Omicron (grey) spike in the presence of the indicated doses of Camostat or E64D, then analysed after 48 hours. % inhibition calculated relative to the maximum luminescent signal for each condition. For each variant and dilution, mean ± SEM is shown for an experiment conducted in duplicate, ****p<0.0001 two sided unpaired t test. **g.** Titration of inhibitors in A549-ACE2-TMPRSS2-based luminescent reporter cells using live virus. Cells were infected at MOI = 0.01 with Delta or Omicron variants in the presence of the indicated doses of Camostat or E64D, then analysed after 24 hours. % inhibition was calculated relative to the maximum luminescent signal for each condition. For each variant and dilution, mean ± SEM is shown for an experiment conducted in triplicate. Data in **f-g** are representative of two independent experiments. **h.** ACE2 and TMPRSS2 mRNA expression by qPCR in human lung tissue (4 pieces of tissue each from upper and lower). Lower – Lung parenchyma Upper - main bronchus. Each data point is the mean of the technical replicates (n=2). Centre line median of biological replicates (n=4 for each lung region); box interquartile range (IQR), whiskers range, two-sided unpaired t test. No adjustments were made for multiple comparisons.

ACCELERATED ARTICLE PREVIEW

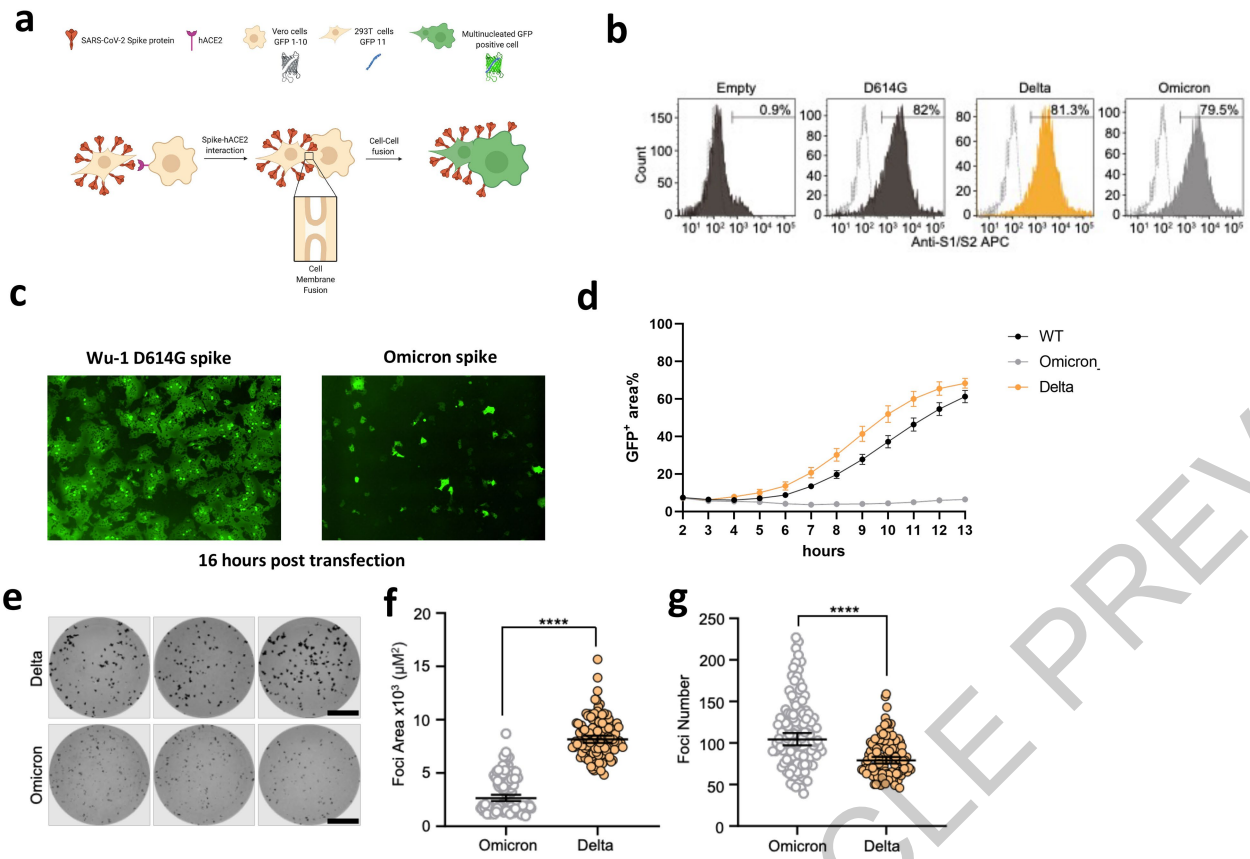

Fig. 4 SARS-CoV-2 Omicron variant spike shows impaired cell-cell fusion activity and smaller infection foci generated by live virus. a. Schematic of cell-cell fusion assay created with BioRender.com. **b.** spike expression at the cell surface as determined by flow cytometry, showing fluorescence intensity distribution histogram (% spike positive cells are indicated) **c.** Reconstructed images at 16 hours of GFP+ syncytia. **d.** Quantification of cell-cell fusion kinetics showing percentage of green area to total cell area over time (WT is Wuhan-1 D614G). Mean is plotted with error bars representing SEM from 8 fields of views at each time point. Data are representative of at least two independent experiments. **e.** Three representative images of 96-well plate wells with infection foci formed by Delta (top row) or Omicron (bottom row) live virus. Bar is 2mm. **f.** Geometric mean and 95% confidence intervals for focus area as determined by ELISpot image analysis for Omicron (n=111 wells) and Delta (n=112 wells). **g.** Focus number per well for the same experiments as **f**. Geometric mean and 95% confidence intervals for focus number per well for Omicron and Delta infections. Two sided p-values **** <0.0001 as determined by the Wilcoxon rank sum test.

ACCELERATED ARTICLE PREVIEW

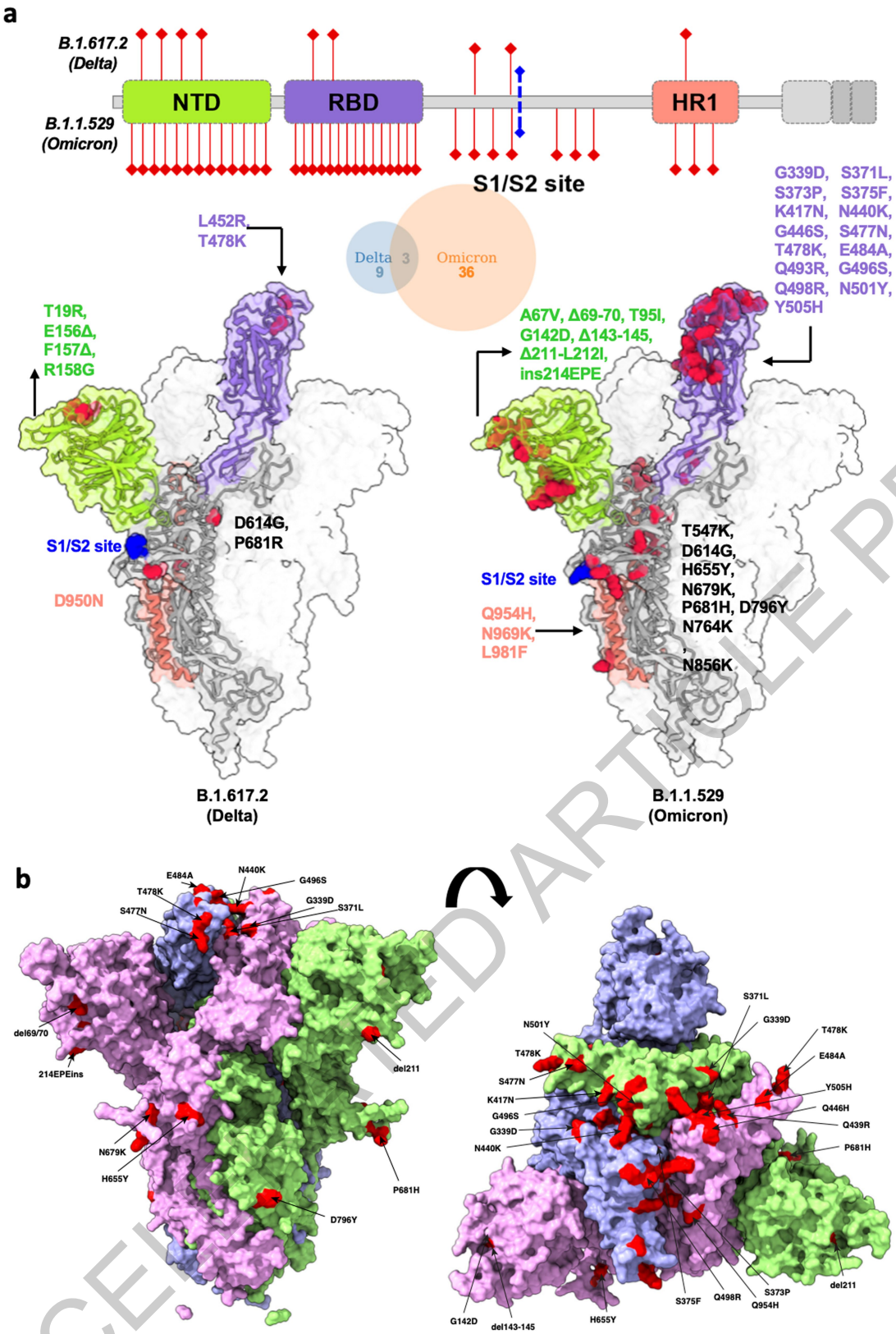

ACCEPTED ARTICLE PREVIEW

Extended Data Fig. 1 Structural model of SARS-CoV-2 Delta and Omicron spike variants. **a.** Variant structures for Delta and Omicron of spike protein displaying mutational sites in red color, generated using the cryo-EM structure PDB# 7A94 as a reference. The schematic highlights differences in domain-wise mutations across protein length. **b.** Side and top down surface representation of the Omicron spike protein**.** Spike homotrimer structures were created predicted *in silico* by the Alphafold2 software package. Individual mutations making up the Omicron spike are highlighted in red on each of the three homotrimers.

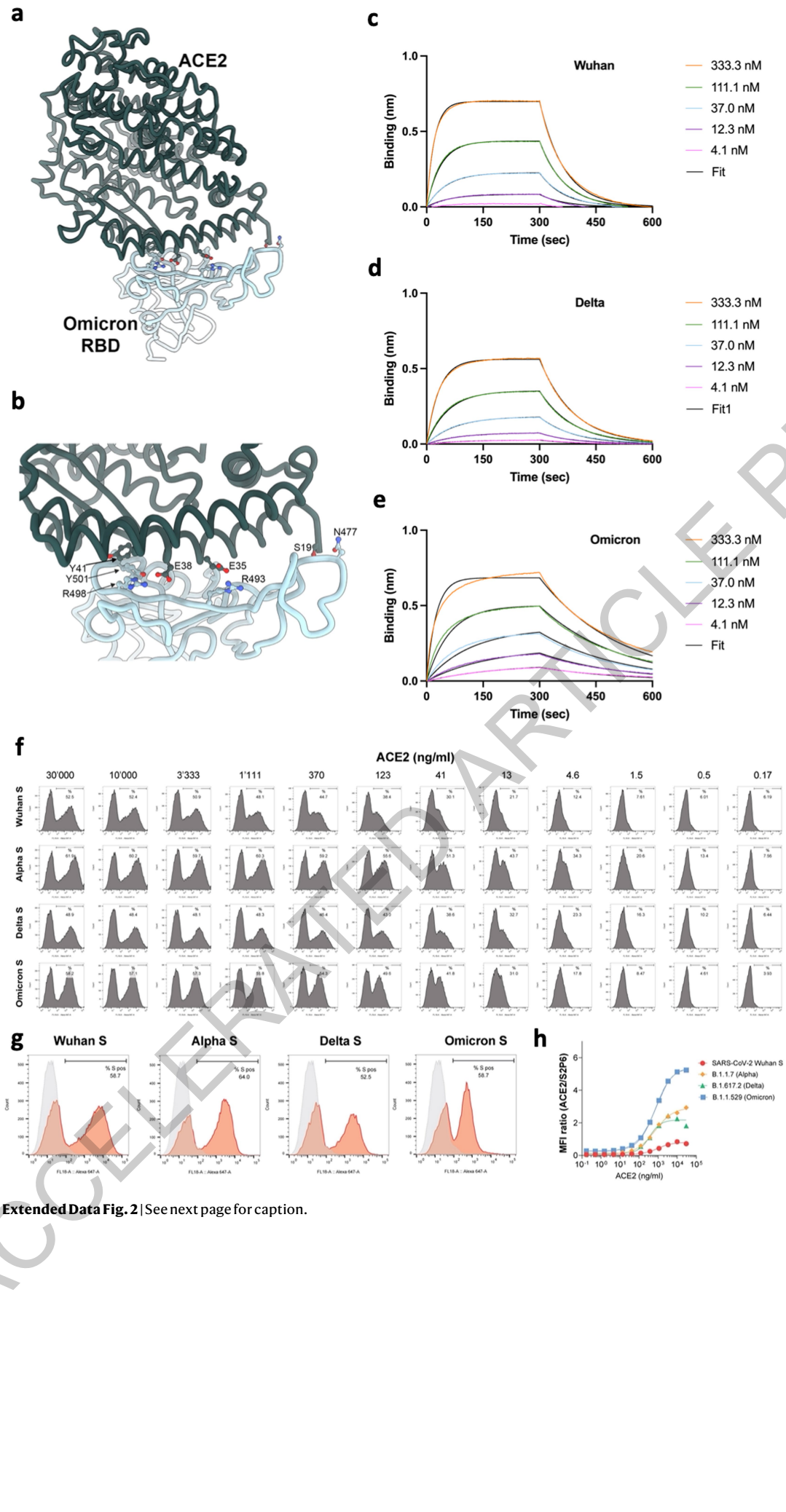

Extended Data Fig. 2 | See next page for caption.

ACCELERATED ARTICLE PREVIEW

Extended Data Fig. 2 Omicron spike binding to ACE2: a. Rendering of the contacts formed between the Omicron RBD (light blue) and human ACE2 (dark green) using PDB 7TN0 described in[16] b. Zoomed-in view showing select amino acid side chains participating in remodeling of interactions between the Omicron RBD and ACE2. c-e. Biolayer interferometry binding analysis of human ACE2 to immobilized SARS-CoV-2 Wuhan-Hu-1 **c.** Delta **d.** or Omicron **e.** RBDs. Black lines correspond to a global fit of the data using a 1:1 binding model. **f.** Flow cytometry analysis of ACE2 binding to SARS-CoV-2 Wuhan, B.1.1.7 (Alpha), B.1.617.2 (Delta) or Omicron (B.1.1.529) spike proteins transiently expressed in ExpiCHO cells. **g.** Expression level of each spike as measured via binding by S2-subunit targeting S2P6 mAb. Grey histograms represent background florescence of cells stained with the secondary antibody only. **h.** Normalized ACE2 binding results based on spike protein expression levels. Values on the Y axis indicate the ratio between the mean fluorescence intensity (MFI) of positive cells stained for ACE2 binding and the MFI of the S2P6 positive cells. Data points in h. are mean of technical triplicates and data shown are representative two independent experiments.

ACCELERATED ARTICLE PREVIEW

a

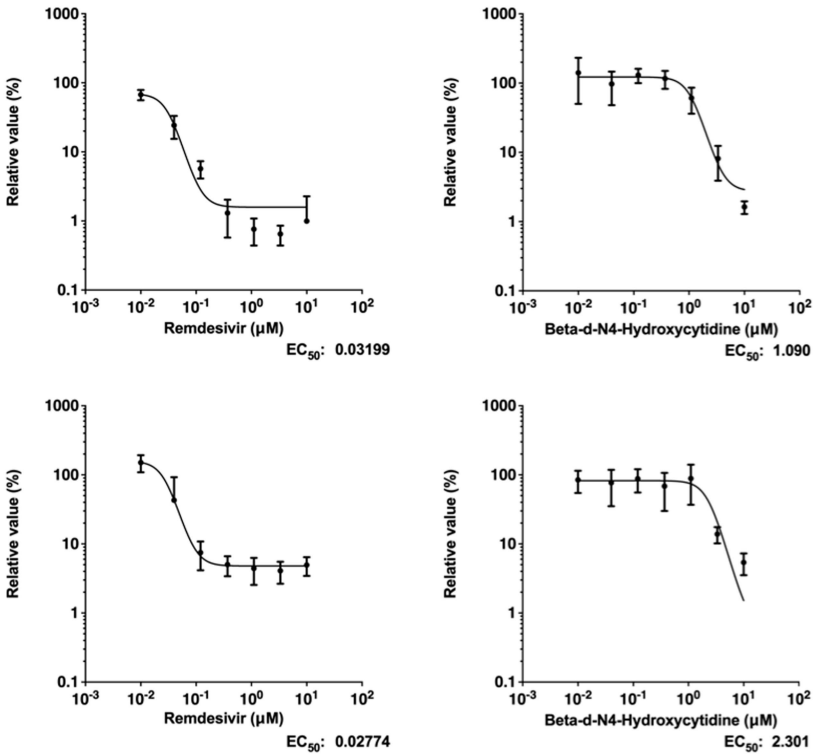

b

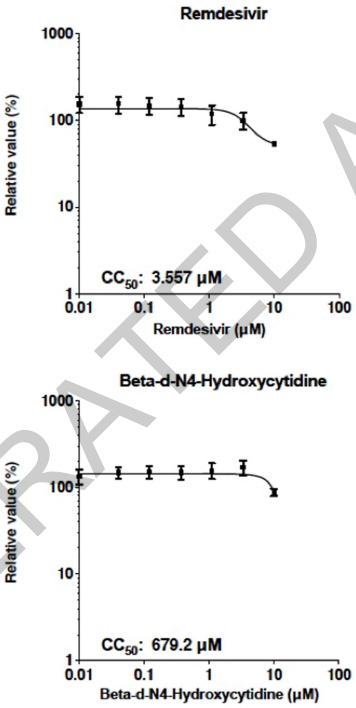

Extended Data Fig. 3 | See next page for caption.

ACCELERATED ARTICLE PREVIEW

Extended Data Fig. 3 Sensitivity of replication competent SARS-CoV-2 Omicron and Delta variants to clinically approved direct acting antiviral molecules remdesivir and the active metabolite of molnupiravir. HOS cells overexpressing ACE2 and TMPRSS2 were used and a viral input of 1000TCID50 was used (TCID50 measured using VeroE6/TMPRSS2 cells). **a.** Dose-response curves. Infection as measured by viral RNA copies relative to the no drug control (100%) is plotted on the y axis with serial drug dilution on the x axis. EC50 is indicated for each panel and calculated in GraphPad Prism. Data points are mean of technical quadruplicates with +/- SEM shown. Curve fitting for dose response was done in GraphPad prism. **b.** toxicity assay showing relative cell viability at a range of drug doses. Data points are mean of technical quadruplicates with +/- SEM shown. All data are representative of two independent experiments.

ACCELERATED ARTICLE PREVIEW

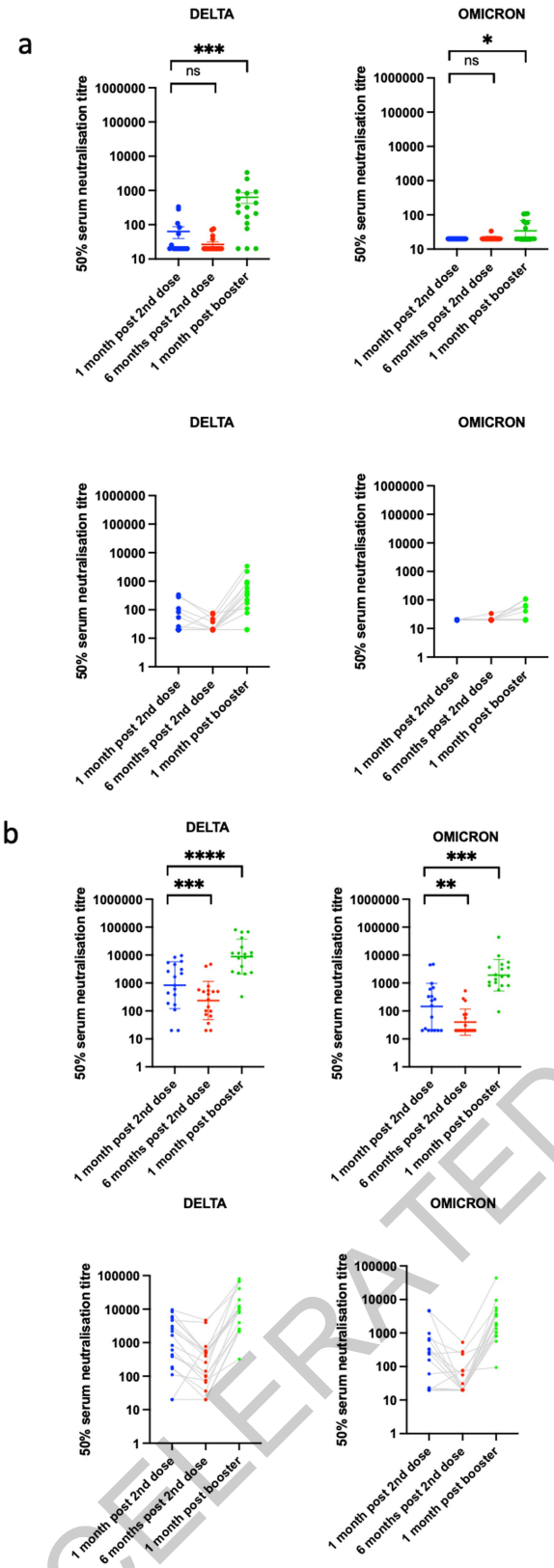

Extended Data Fig. 4 Neutralisation of spike pseudotyped virus by sera from vaccinated individuals over three time points following dose two (ChAdOx-1 or BNT162b2) and dose three (BNT162b2 only) **a**. n=17 ChAdOx-1 or **b.** n=18 BNT12b2. GMT (geometric mean titre) shown as a line with s.d as bars are presented. Data representative of two independent experiments each with two technical replicates. **p<0.01, *** p<0.001, ****p<0.0001 Wilcoxon matched-pairs signed rank test, ns not significant, two-sided. Data are for individuals who tested negative for anti-N IgG at each time point.

ACCELERATED ARTICLE PREVIEW

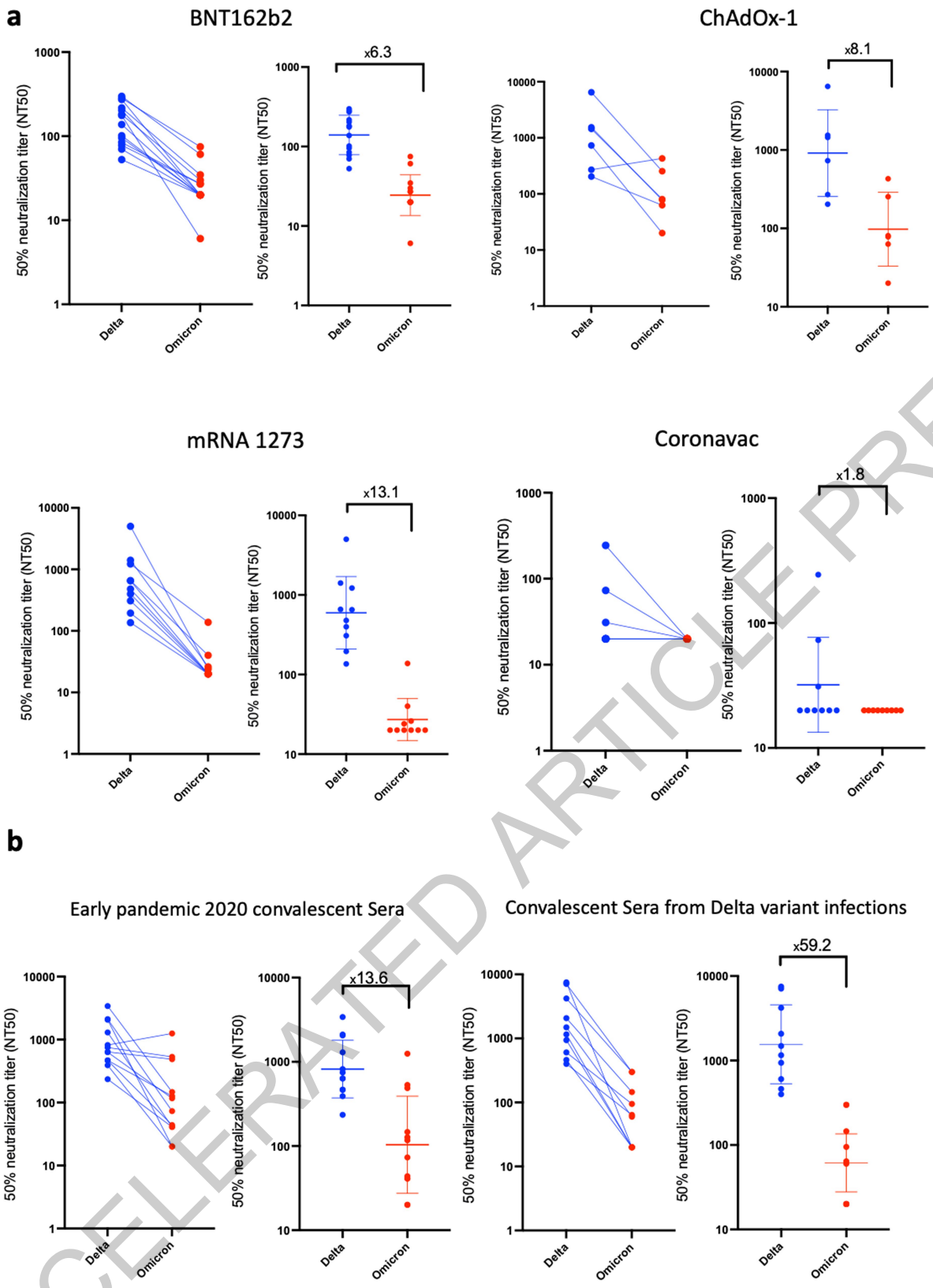

ACCELERATED ARTICLE PREVIEW

Extended Data Fig. 5 Live virus neutralization by vaccine-elicited and convalescent sera

a. Neutralisation of replication competent Delta and Omicron viruses by sera from vaccinated individuals following dose two of ChAdOx-1 (n=5), BNT162b2 (n=10), mRNA 1273(n=10) , and Coronavac (n=9) vaccines**. b.** neutralization of live viruses by sera derived from recovered individuals following infection in early 2020 or with confirmed Delta infection. GMT (geometric mean titre) of three technical replicates are shown as a line with s.d as bars are presented. Data representative of two independent experiments. Fold change in NT50 is indicated.

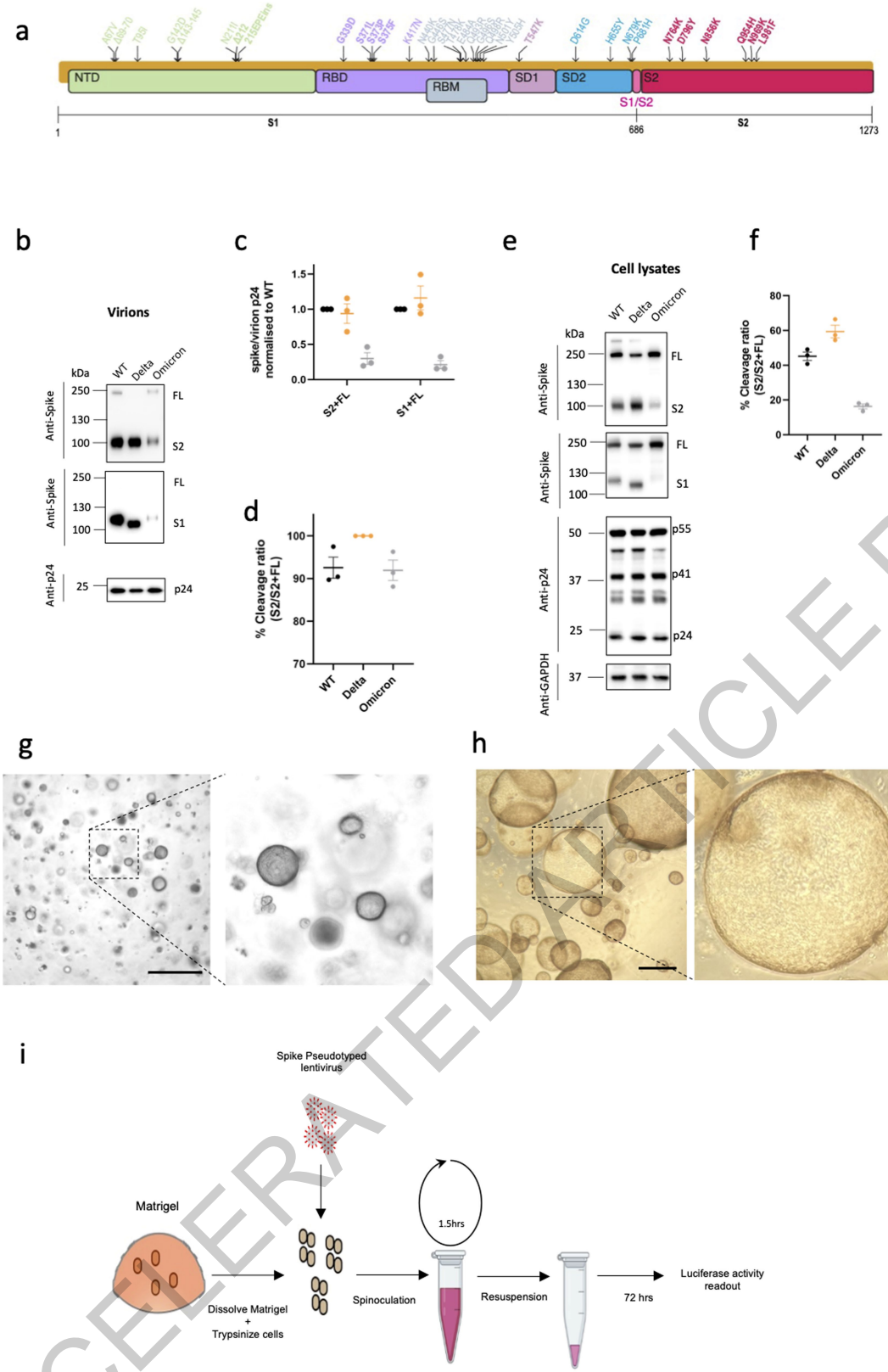

Extended Data Fig. 6 | See next page for caption.

ACCELERATED ARTICLE PREVIEW

Extended Data Fig. 6 SARS-CoV-2 Omicron Variant spike pseudotyped lentiviruses

a. Graphical representation of Omicron spike mutations present in expression plasmid used to generate lentiviral pseudotyped virus (PV). Mutations coloured according to location in spike; bold mutations are novel to this lineage and have not been identified in previous variants of concern (VOCs). **b.** western blots of pseudotyped virus (PV) virions from 293T producer cells following transfection with plasmids expressing lentiviral vectors and SARS-CoV-2 S plasmids. (WT- Wuhan-1 with D614G), probed with antibodies for HIV-1 p24 and SARS-Cov-2 S2 (top) and S1 (bottom). **c-d.** quantification of western blots showing **c**. ratio of spike:p24 in virions, **d**. ratio of S2:total spike**.** Mean ratio +/- sd is shown for 3 biological replicates **e.** Western blot of cell lysates used to produce virions with **f**. quantification of S2 to total spike ratio. Mean ratio +/- sd is shown for 3 biological replicates **g.** brightfield images of lower airway organoids **h**. brightfield images of of cholangiocyte organoids (Scale bars 200 **μ**m). **i.** infection schematic for entry assays in organoids created with BioRender.com.

ACCELERATED ARTICLE PREVIEW

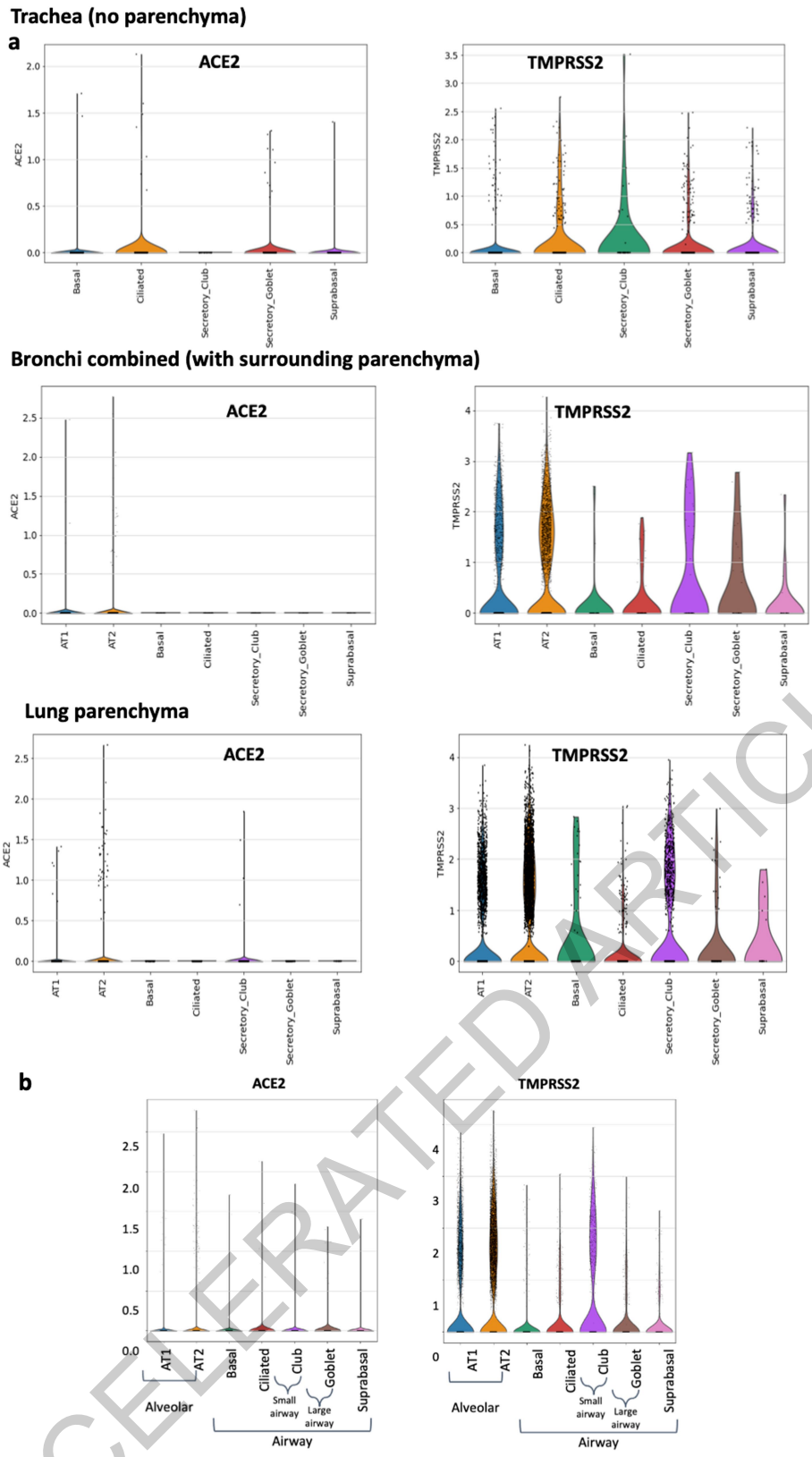

Extended Data Fig. 7 ACE2 and TMPRSS2 tissue expression levels by single cell RNAseq a. Log-normalised expression of ACE2 and TMPRSS2 genes in single-nuclei RNAseq data for indicated tissue types and. **b.** Log-normalised aggregrated expression of ACE2 and TMPRSS2 genes in single-nuclei RNAseq data from human alveolar (AT1 - alveolar type 1, AT2 - alveolar type 2 pneumocytes), and airway epithelial cells (basal, suprabasal, goblet and ciliated). Data are derived from in Madissoon et al.

ACCELERATED ARTICLE PREVIEW

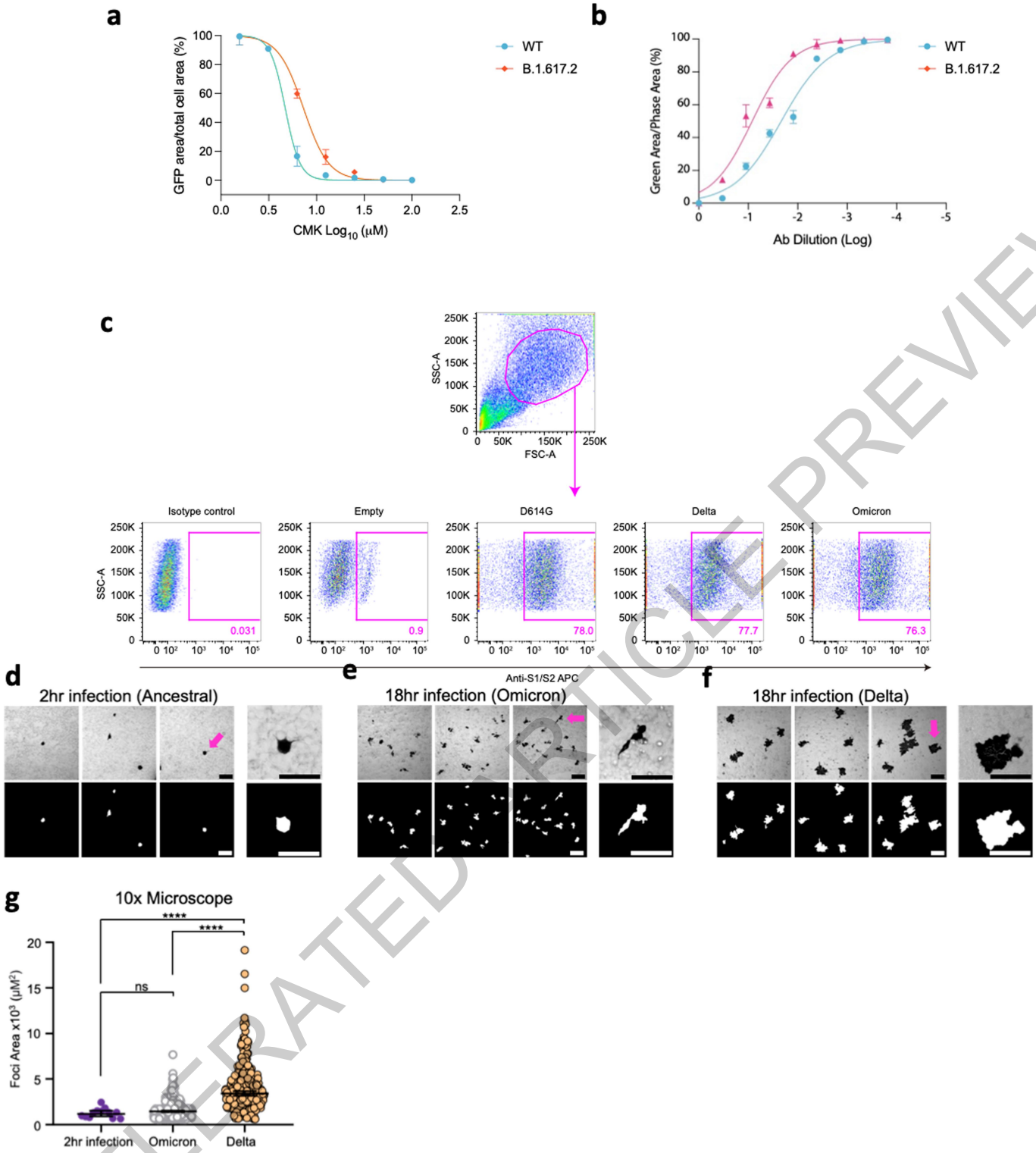

Extended Data Fig. 8 | See next page for caption.

ACCELERATED ARTICLE PREVIEW

Extended Data Fig. 8 SARS-CoV-2 cell-cell fusion and infection focus formation. a. effect of furin inhibition using CMK on cell-cell fusion for WT (Wuhan-1 D614G) and Delta variant. CMK drug dilution indicated on x axis and fusion on y axis. Quantification of cell-cell fusion shows percentage of green area to total cell area. Mean of technical replicates is plotted with error bars representing SEM. Data are representative of at least two independent experiments. b. impact of neutralising antibodies from UK wave one 2020 sera on cell-cell fusion for WT (Wuhan-1 D614G) and Delta variant. Serial dilutions of sera added to acceptor cells before co-cultivation with donor cells. Data points are mean of technical replicates is plotted with error bars representing SEM. c. Gating strategy for cell surface staining of SARS-CoV-2 spike proteins from 293T cells transfected with plasmids expressing spike, using rabbit anti-SARS-CoV-2 spike S1/2 polyclonal antibody at 1:100. d-g. Omicron shows attenuated localized spread compared to Delta. d. Microscope images of foci (pink arrow) 2 hours post-infection with ancestral SARS-CoV-2. Bar is 200 microns. e. Images of Omicron foci 18 hours post-infection. f. Images of Delta foci 18 hours post-infection g. Geometric mean and 95% confidence intervals of focus area of microscope images of 2 hours post-ancestral infection (n=12 foci, purple), 18 hours post-Omicron infection (n=363, grey), and 18 hours post-Delta infection (n=275, orange). p-values are not significant (ns) or **** <0.0001 as determined by two sided Wilcoxon rank sum test.

ACCELERATED ARTICLE PREVIEW

Extended Data Table 1 Kinetic Analysis of human ACE2 binding to SARS-CoV-2 VOC by Biolayer Interferometry.

	Wuhan	Delta	Omicron
KD (nM)	127	190	44
k_{on} (M^{-1} s^{-1})	1.1×10^{5}	5.9×10^{4}	1.1×10^{5}
k_{off} (s^{-1})	1.4×10^{-2}	1.1×10^{-2}	4.7×10^{-3}

Values reported represent the global fit to the data shown in Extended Data Figure 2.

ACCELERATED ARTICLE PREVIEW

Extended Data Table 2 Demographic characteristics of participants in longitudinal vaccine elicited sera neutralisation study.

Characteristic	Total	Pfizer (BNT162b2)	AstraZeneca (ChAdOx1)
Total number, n (%)	40	20 (50)	20 (50)
Age, median years (IQR)	70.5 (62.5, 74.0)	71.0 (55.8, 75.8)	69.5 (63.0, 73.8)
≥80, n (%)	4 (10)	4 (20)	0 (0)
<80, n (%)	36 (90)	16 (80)	20 (100)
Gender, n (%)			
Male	15 (37.5)	8 (40)	7 (35)
Female	25 (62.5)	12 (60)	13 (65)
Previous COVID-19			
Yes	5 (12.5)	2 (10)	3 (15)
No	35 (87.5)	18 (90)	17 (85)
Type of booster			
Moderna	3 (7.5)	0	3 (15)
Pfizer	37 (92.5)	20 (100)	17 (85)
Duration between booster dose and sampling, median days (IQR)	34 (32, 36)	34.0 (32.0, 36.0)	33.5 (30.3, 35.8)

Data relate to participants in Figure 1 and Extended Data Figure 4. Categorical variables (expressed as proportions and percentages) and continuous variables (expressed as medians with inter quartile ranges [IQR]) are shown.

ACCELERATED ARTICLE PREVIEW

nature portfolio

Corresponding author(s): Sato, Gupta

Last updated by author(s): Dec 24, 2021

Reporting Summary

Nature Portfolio wishes to improve the reproducibility of the work that we publish. This form provides structure for consistency and transparency in reporting. For further information on Nature Portfolio policies, see our Editorial Policies and the Editorial Policy Checklist.

Statistics

For all statistical analyses, confirm that the following items are present in the figure legend, table legend, main text, or Methods section.

n/a	Confirmed	
☐	☒	The exact sample size (*n*) for each experimental group/condition, given as a discrete number and unit of measurement
☐	☒	A statement on whether measurements were taken from distinct samples or whether the same sample was measured repeatedly
☐	☒	The statistical test(s) used AND whether they are one- or two-sided *Only common tests should be described solely by name; describe more complex techniques in the Methods section.*
☒	☐	A description of all covariates tested
☒	☐	A description of any assumptions or corrections, such as tests of normality and adjustment for multiple comparisons
☐	☒	A full description of the statistical parameters including central tendency (e.g. means) or other basic estimates (e.g. regression coefficient) AND variation (e.g. standard deviation) or associated estimates of uncertainty (e.g. confidence intervals)
☐	☒	For null hypothesis testing, the test statistic (e.g. *F*, *t*, *r*) with confidence intervals, effect sizes, degrees of freedom and *P* value noted *Give P values as exact values whenever suitable.*
☒	☐	For Bayesian analysis, information on the choice of priors and Markov chain Monte Carlo settings
☒	☐	For hierarchical and complex designs, identification of the appropriate level for tests and full reporting of outcomes
☐	☒	Estimates of effect sizes (e.g. Cohen's *d*, Pearson's *r*), indicating how they were calculated

Our web collection on statistics for biologists contains articles on many of the points above.

Software and code

Policy information about availability of computer code

Data collection	*Provide a description of all commercial, open source and custom code used to collect the data in this study, specifying the version used OR state that no software was used.*
Data analysis	Prism 9, Excel, GROMACS2018; FloJo, Fiji (v1.49) software, ImageJ, geneious prime, scanpy, Alphafold, GISAID and EpiCoV websites

For manuscripts utilizing custom algorithms or software that are central to the research but not yet described in published literature, software must be made available to editors and reviewers. We strongly encourage code deposition in a community repository (e.g. GitHub). See the Nature Portfolio guidelines for submitting code & software for further information.

Data

Policy information about availability of data

All manuscripts must include a data availability statement. This statement should provide the following information, where applicable:

- Accession codes, unique identifiers, or web links for publicly available datasets
- A description of any restrictions on data availability
- For clinical datasets or third party data, please ensure that the statement adheres to our policy

The raw data in this study are available from the corresponding authors with no restrictions upon reasonable request.

Field-specific reporting

Please select the one below that is the best fit for your research. If you are not sure, read the appropriate sections before making your selection.

☒ Life sciences ☐ Behavioural & social sciences ☐ Ecological, evolutionary & environmental sciences

For a reference copy of the document with all sections, see nature.com/documents/nr-reporting-summary-flat.pdf

Life sciences study design

All studies must disclose on these points even when the disclosure is negative.

Sample size	Our sample sizes were based on our previous in vitro SARS-CoV-2 work, and based on practical availability of sera from participants.
Data exclusions	Individuals positive for N antibody were excluded from analysis in neutralisation experiments and data with and without the exclusions are presented in the figures
Replication	experiments were done at least twice as biological replicates
Randomization	we did not use randomisation in our lab experimental designs
Blinding	we did not use blinding in our lab experimental designs

Reporting for specific materials, systems and methods

We require information from authors about some types of materials, experimental systems and methods used in many studies. Here, indicate whether each material, system or method listed is relevant to your study. If you are not sure if a list item applies to your research, read the appropriate section before selecting a response.

Materials & experimental systems

n/a	Involved in the study
☐	☒ Antibodies
☐	☒ Eukaryotic cell lines
☒	☐ Palaeontology and archaeology
☒	☐ Animals and other organisms
☐	☒ Human research participants
☒	☐ Clinical data
☒	☐ Dual use research of concern

Methods

n/a	Involved in the study
☒	☐ ChIP-seq
☐	☒ Flow cytometry
☒	☐ MRI-based neuroimaging

Antibodies

Antibodies used

For Western blot:
Rabbit anti-SARS-CoV-2 S polyclonal antibody (PA1-41165, Thermofisher, 1:2,000),
Rabbit anti-SARS-CoV-2 N monoclonal antibody (clone HL344, GeneTex, Cat# GTX635679, 1:2,000),
Mouse anti-SARS-CoV-2 S1 monoclonal antibody (MAB105403, R&D systems, 1:2,000),
Rabbit anti-GAPDH polyclonal antibody (10494-1-AP, Proteintech, 1:5,000),
Mouse anti-HIV p24 monoclonal antibody (NIBSC, ARP313, 1:20,000)
Horseradish peroxidase (HRP)-conjugated Goat anti-rabbit IgG antibody (Cell Signaling, 7074, 1:5,000),
HRP-conjugated anti-mouse IgG antibody (Cell Signaling, 7076, 1:5,000).

For neutralisation assay:
Casirivimab and Imdevimab

For IF
Mouse anti-SARS-CoV-2 Spike monoclonal antibody (clone1A9, GeneTex, GTX632604,)
anti-GM130[EP892Y]-cis-Golgi (ab52649, 1:250)
phalloidin 647 (Thermofisher, A22287, 1:1000)
Goat anti-Rabbit IgG (H+L) Cross-Adsorbed Secondary Antibody, Alexa Fluor 594 (Thermofisher, A-11012, 1:1,000)
Goat anti-Mouse IgG (H+L) Cross-Adsorbed Secondary Antibody, Alexa Fluor 488 (Thermofisher, A-11001, 1:1,000)

For FACS
Alexa Fluor647 Goat Anti-Human IgG secondary Ab (1.5 mg/ml) (Jackson Immunoresearch)
rabbit anti-SARS-CoV-2 S S1/S2 polyclonal antibody (Thermo Fisher Scientific, Cat# PA5-112048, 1:100).
Normal rabbit IgG (SouthernBiotech, Cat# 0111-01, 1:100)
APC-conjugated goat anti-rabbit IgG polyclonal antibody (Jackson ImmunoResearch, Cat# 111-136-144, 1:50)

Validation

Rabbit anti-SARS-CoV-2 S polyclonal antibody (PA1-41165, Thermofisher, 1:2,000),
Rabbit anti-SARS-CoV-2 N monoclonal antibody (clone HL344, GeneTex, Cat# GTX635679, 1:2,000),
Mouse anti-SARS-CoV-2 S1 monoclonal antibody (MAB105403, R&D systems, 1:2,000),
These products were validated by putting negative controls of the antigens in western blotting. We verified that the bands detected at appropriated sizes were not observed in the samples from the antigen-negative cells.

Rabbit anti-GAPDH polyclonal antibody (10494-1-AP, Proteintech, 1:5,000). This antibody has been tested as stated on the supplier's website in human placenta tissue, Raji cells, HepG2 cells, K-562 cells, mouse heart tissue, A549 cells, PC-13 cells, arabidopsis whole plant tissue, corn whole plant tissue, mouse brain tissue, HEK-293 cells, HeLa cells, rat brain tissue, mouse skin tissue, RAW 264.7 cells, C6 cells, Jurkat cells, NIH/3T3 cells

Horseradish peroxidase (HRP)-conjugated Goat anti-rabbit IgG antibody (Cell Signaling, 7074, 1:5,000),
HRP-conjugated anti-mouse IgG antibody (Cell Signaling, 7076, 1:5,000).
Alexa Fluor647 Goat Anti-Human IgG secondary Ab (1.5 mg/ml) (Jackson Immunoresearch)
anti-GM130[EP892Y]-cis-Golgi (ab52649, 1:250)
phalloidin 647 (Thermofisher, A22287, 1:1000)
Goat anti-Rabbit IgG (H+L) Cross-Adsorbed Secondary Antibody, Alexa Fluor 594 (Thermofisher, A-11012, 1:1,000)
Goat anti-Mouse IgG (H+L) Cross-Adsorbed Secondary Antibody, Alexa Fluor 488 (Thermofisher, A-11001, 1:1,000)
These products were thoroughly validated by the providers and work optimally with the protocol for Western blotting or FACS or IF, as described in the Method section. We ensured the results are accurate and reproducible.

Casirivimab and Imdevimab were generated as described in the Method section. The nucleotide sequences of their templates were verified by Sanger sequencing.

Eukaryotic cell lines

Policy information about cell lines

Cell line source(s)

HEK293T cells (a human embryonic kidney cell line; ATCC CRL-3216)
HOS-ACE2/TMPRSS2 cells (HOS cells stably expressing human ACE2 and TMPRESS2) (Saito et al., Nature, 2021)
VeroE6/TMPRSS2 cells [an African green monkey (Chlorocebus sabaeus) kidney cell line; JCRB1819]
Calu-3 cells (a human lung epithelial cell line; ATCC HTB-55 or a gift from Paul Lehner)
H1299 a gift from Simon Cook
HeLa-ACE2 a gift from James Voss
CaCo2 a gift from Ian Goodfellow
A549-ACE2/TMPRSS2 from Massimo Palmarini
293T (CRL-3216)
293T-ACE2/TMPRSS2, 293T-ACE2ΔTMPRSS2, 293T-TMPRSS2, 293T-GFP11 and Vero -GFP1-10 were provided by Leo James
Vero-ACE2/TMPRSS2 from Emma Thomson
ExpiCHO cells from Davide Corti
A549-ACE2-TMPRSS2-based luminescent reporter cells from Nick Matheson

Authentication

HEK293T cells, H1299 and Calu-3 cells were authenticated by ATCC.
VeroE6/TMPRSS2 cells was authenticated by JCRB Cell Bank.
HOS-ACE2/TMPRSS2 cells Saito et al., Nature, 2021) was not authenticated.

Mycoplasma contamination

All cell lines were regularly tested for mycoplasma contamination by using PCR and were confirmed to be mycoplasma-free.

Commonly misidentified lines
(See ICLAC register)

No commonly misidentified cell lines were used.

Human research participants

Policy information about studies involving human research participants

Population characteristics

Vaccine sera were collected from fourteen vaccinees four weeks after the second vaccination with BNT162b2 (Pfizer-BioNTech) (average age: 46, range: 38-55, 21% male),

ten vaccinees four weeks after the second vaccination with mRNA-1273 (Moderna) (average age: 26, range: 21-37, 40% male),

nine vaccinees 4-6 weeks after the second vaccination with CoronaVac (Sinovac) (44% male).

Delta convalescent Delta sera were collected from ten vaccine-naive individuals who had infected with Delta variant (B.1.617.2 or AY.29) (average age: 46, range: 22-63, 70% male).

Recruitment

The voluntary donors were recruited at Kyoto University (BNT162b2 and mRNA-1273 vaccinees),

Universidad San Francisco de Quito (CoronaVac vaccinees),

	Kuramochi Clinic Interpark (Delta convalescents) regardless of age, sex, gender, race, ethnicity, or other characteristics. Written informed consent was obtained from the voluntary donor. Community vaccinated articipants were also recruited by the NIHR Cambridge Bioresource
Ethics oversight	All protocols involving specimens from human subjects recruited at Kyoto University, Kuramochi Clinic Interpark Universidad San Francisco de Quito were reviewed and approved by the Institutional Review Boards of Kyoto University (approval ID: G0697), Kuramochi Clinic Interpark (approval ID: G2021-004) Universidad San Francisco de Quito (approval ID: CEISH P2020-022IN), and the Ecuadorian Ministry of Health (approval IDs: MSP-CGDES-2020-0121-O and MSP-CGDES-061-2020). Ethical approval for study of vaccine elicited antibodies in sera from vaccinees was obtained from the East of England – Cambridge Central Research Ethics Committee Cambridge (REC ref: 17/EE/0025). Ethical approval for use of human tissue for measurement of ACE2 and TMPRSS2 levels was obtained as follows: the samples of human upper and lower airways were obtained from the lungs of a multiorgan donor whose lungs were deemed unsuitable for clinical transplantation and after their next of kin consented to their use in research. The studies using human donor lungs tissue were approved by National Research Ethics Committee (NREC) 16/NE/0230.

Note that full information on the approval of the study protocol must also be provided in the manuscript.

Flow Cytometry

Plots

Confirm that:

☒ The axis labels state the marker and fluorochrome used (e.g. CD4-FITC).

☒ The axis scales are clearly visible. Include numbers along axes only for bottom left plot of group (a 'group' is an analysis of identical markers).

☒ All plots are contour plots with outliers or pseudocolor plots.

☒ A numerical value for number of cells or percentage (with statistics) is provided.

Methodology

Sample preparation	HEK293 cells were cotransfected with 400 ng of D614G S or D614G/P681R expression plasmids and 400 ng pDSP1-7 using TransIT-LT1 (Takara, Cat# MIR2300).
Instrument	FACS Canto II instrument (BD Biosciences)
Software	FlowJo
Cell population abundance	n/a (cell sorting was not conducted)
Gating strategy	Extended Data Fig. 8. The cells were gated in the FSC/SSC plot, then the mean fluorescence intensity of surface S protein (APC) was measured. The boundary between S-positive and S-negative was defined by using the cells that the S-expression plasmid was not transfected (i.e., S-negative cells).

☒ Tick this box to confirm that a figure exemplifying the gating strategy is provided in the Supplementary Information.